Assessing spatial and temporal variability of phytoplankton communities' composition in the Iroise Sea ecosystem (Brittany, France): A 3D modeling approach
Part 2: Linking summer mesoscale distribution of phenotypic diversity to hydrodynamism

Mathilde Cadier [a,*], Marc Sourisseau [b], Thomas Gorgues [c], Christopher A. Edwards [d], Laurent Memery [a]

[a] Laboratoire des Sciences de l'Environnement Marin, UMR CNRS/IFREMER/IRD/UBO, 6539 Plouzané, France
[b] Département Dynamiques de l'Environnement Côtier/PELAGOS, Ifremer Centre de Brest, Plouzané, France
[c] Laboratoire d'Océanographie Physique et Spatiale, UMR CNRS/IFREMER/IRD/UBO, 6523, Ifremer, Centre de Brest, Plouzané, France
[d] Institute of Marine Sciences, University of California, Santa Cruz, CA 95064, USA

ARTICLE INFO

ABSTRACT

Tidal front ecosystems are especially dynamic environments usually characterized by high phytoplankton biomass and high primary production. However, the description of functional microbial diversity occurring in these regions remains only partially documented. In this article, we use a numerical model, simulating a large number of phytoplankton phenotypes to explore the three-dimensional spatial patterns of phytoplankton abundance and diversity in the Iroise Sea (western Brittany). Our results suggest that, in boreal summer, a seasonally marked tidal front shapes the phytoplankton species richness. A diversity maximum is found in the surface mixed layer located slightly west of the tidal front (i.e., not strictly co-localized with high biomass concentrations) which separates tidally mixed from stratified waters. Differences in phenotypic composition between sub-regions with distinct hydrodynamic regimes (defined by vertical mixing, nutrients gradients and light penetration) are discussed. Local growth and/or physical transport of phytoplankton phenotypes are shown to explain our simulated diversity distribution. We find that a large fraction (64%) of phenotypes present during the considered period of September are ubiquitous, found in the frontal area and on both sides of the front (i.e., over the full simulated domain). The frontal area does not exhibit significant differences between its community composition and that of either the well-mixed region or an offshore Deep Chlorophyll Maximum (DCM). Only three phenotypes (out of 77) specifically grow locally and are found at substantial concentration only in the surface diversity maximum. Thus, this diversity maximum is composed of a combination of ubiquitous phenotypes with specific picoplankton deriving from offshore, stratified waters (including specific phenotypes from both the surface and the DCM) and imported through physical transport, completed by a few local phenotypes. These results are discussed in light of the three-dimensional general circulation at frontal interfaces. Processes identified by this study are likely to be common in tidal front environments and may be generalized to other shallow, tidally mixed environments worldwide.

© 2017 Published by Elsevier B.V.

1. Introduction

Marine phytoplankton play a key role as the first link in ocean food webs, producing almost 50% of the Earth's annual net primary production (Field et al., 1998). In every location of the ocean, a large number of photoautotrophic species, both prokaryotic and eukaryotic (Falkowski et al., 2004), with very diverse genetic, taxonomic or functional characteristics generally coexists and contributes to biological production at higher trophic levels. The maintenance of high biological diversity is crucial to ensure resilience of ecosystem functioning (Ptacnik et al., 2008) as it allows complementarity between species or taxa to efficiently access heterogeneously distributed resources (Chisholm, 1992). Coexistence between phenotypes having various physiological and functional traits is enabled by several top-down or bottom-up complementary mechanisms. An example of top-down control is the regulation of primary producers' diversity by herbivorous consumers (i.e., zooplankton) that adjust their predation to the most

abundant prey (e.g., through prey selectivity as described in Chase et al., 2002 and Hillebrand et al., 2007). On the other hand, bottom-up control can occur through ecological processes of adaptation (i.e. selection of optimal traits within evolutionary mutational changes), acclimation (i.e. phenotypic plasticity) enabling species locally adapted to environmental conditions to thrive and exclusive competition. As long as the residence time of water masses is sufficiently long (i.e., quasi steady state), this last process occurs, benefiting species with the highest fitness with a negative impact on the diversity. Indeed, following resource competition theory (Tilman, 1977, 1982), species with the lowest positive equilibrium resource concentration R^* (which measures the fitness of each phenotypes) outcompete other, less locally adapted organisms over time. This process of natural selection (bottom up control) could lead to diversity decline. However, high variability in environmental conditions at timescales similar to phytoplankton ecological rates can prevent complete exclusion and contributes to the maintenance of high diversity levels (Hutchinson, 1961; Sommer, 1984; Huston, 1979; Huisman and Weissing, 2001; Scheffer et al., 2003).

Local ecological processes alone are not sufficient to explain observed diversity patterns in the ocean. Indeed, apart from modulating the background environmental conditions, physical processes also noticeably gather phytoplankton types from different regions through advective transport by ocean currents combined with mixing that yields dispersion. The contemporaneous disequilibrium framework (Richerson et al., 1970) suggests that dispersal in a dynamic ocean contributes to maintain low fitness phenotypes in significant proportion by preventing the system from reaching a stable equilibrium. Indeed, as described by MacArthur and Wilson (1967), passive movements of species by physical transport associated with mixing have the potential to significantly affect qualitative and quantitative measures of local diversity by combining properties from different regions.

According to the neutral theory of biodiversity (Hubbell, 2001), the fate of species that are considered to be equivalent in terms of fitness is locally governed by stochastic processes (ecological drift) rather than determined by environmental traits selection. In contrast with niche segregation theory and resource competition, the observed diversity patterns would therefore be primarily explained by replenishment or discharge of local species pool through physical dynamics. Processes of local growth, exclusive competition and physical dispersal all shape the ocean diversity landscape and interact such that their individual impact depends on their relative timescale (Clayton et al., 2013).

At the global scale, marine microbial diversity has been explored through several field studies (Hillebrand, 2004; Irigoien et al., 2004; Pommier et al., 2007; Fuhrman et al., 2008) and modeling efforts (Barton et al., 2010). Species richness varies with latitude, generally decreasing from tropics to poles (corresponding to a low to high environmental variability). Also, it has been shown that dynamical transport contributes to higher local diversity (α) by decreasing the differences between distinct oceanic regions in terms of phytoplankton community composition (Clayton et al., 2013; Levy et al., 2014). Thus, local and regional diversity patterns are strongly influenced by large-scale diversity (Ricklefs, 1987). Transport over about a hundred kilometers is sufficient and acts sufficiently rapidly to significantly shape the diversity of planktonic ecosystems at local scales (Adjou et al., 2012).

At a more regional scale, physical dynamics induced by the presence of time-evolving mesoscale (10–100 km) structures with a lifetime of the same order of magnitude as phytoplankton generation timescales (D'Ovidio et al., 2010) also impact the regional diversity landscape in many distinct ways. Indeed, besides passive stirring of organisms between physical regimes, these structures may create ecological niches through variability in nutrient supply (Sedigh Marvasti et al., 2016), resulting in heterogeneously distributed primary producers' abundance, total chlorophyll (Gaube et al., 2014) and diversity patterns (McGillicuddy and Dennis, 2016). Uptakes rates, primary production (Levy et al., 2001; Rivière and Pondaven, 2006) and carbon export (Sharples, 2008) are likewise affected by mesoscale eddies and fronts.

Because the lifetime of eddies or vortices is longer than a few days, water masses in their interiors remain isolated and could act as shelters for less-fit species (Bracco et al., 2000; Perruche et al., 2010) whereas their edges and other frontal interfaces are generally more diverse than surrounding areas (Lévy et al., 2015) for two complementary reasons. High biomass associated with widely diversified plankton communities at frontal interfaces are then explained by (i) the encounter of water masses from both sides of the front (Perruche et al., 2010) potentially increasing the number of different species coexisting locally at the interface and (ii) the local growth of opportunistic fast growing phenotypes which may be enabled by vertical mixing and a net upward nutrient flux into the euphotic layer (Levin and Paine, 1974; Claustre et al., 1994; Barton et al., 2014).

However, the relative importance of these two complementary mechanisms (passive transport and local growth) on high diversity at fronts has not been effectively tested. Here, we explore how much phenotypic diversity in phytoplankton can be sustained by lateral and vertical advection and/or mixing relative to local growth in a highly dynamic tidal front environment with heterogeneous growth conditions including both spatial and temporal variability. To answer this question, we use a coupled physical/biogeochemical model including a large number of phytoplankton phenotypes which are differentiated by their optimal growth conditions (temperature, nutrient and light) and therefore compete for resources while they are consumed by zooplankton grazers and carried by currents.

This modeling setup is applied to the Ushant Front ecosystem of the Iroise Sea. The Ushant front is characterized by a sharp horizontal temperature gradient of 2 °C·km^{-1} (Mariette, 1983) associated with high chlorophyll concentration during summer, from May to October (Le Boyer et al., 2009). Its position, located roughly where the 15 °C surface temperature isotherm intersects the surface (Fig. 1), oscillates with different time frequencies, varying from seasonal to bi-weekly and semi-diurnal periods according to tidal fluctuations and annual forcing variations. Observed high phytoplankton biomass in the vicinity of the front location has been shown to be related to a local increase of inorganic nutrients (Savidge, 1976). In this study, we use the model to investigate underlying processes contributing to biomass and phenotypic diversity patterns at the front. We specifically examine interactions between phenotypes competing for light and macronutrients in this very dynamic frontal environment. We aim to quantify the relative roles of local ecological processes and physical transport in shaping the diversity of this frontal ecosystem.
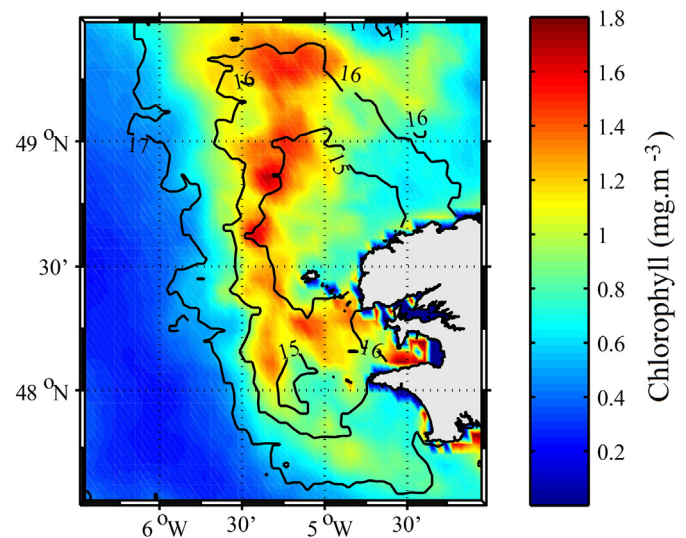

Fig. 1. Surface chlorophyll in September 2007, computed from SeaWifs satellite observations, following Gohin et al. (2002). Black contour line represents Sea Surface Temperature from MODIS.

2. Method

We use a three dimensional numerical physical-biogeochemical model to describe the distribution of a large number of phytoplankton phenotypes across the Ushant Front during a summer period. The simulations conducted in this study use the exact same set-up as presented in Cadier et al., 2017.

2.1. Physical model

A configuration of the ROMS-AGRIF model (Shchepetkin and McWilliams, 2005; Penven et al., 2006), commonly used for regional investigations (e.g. Echevin et al., 2008; Auger et al., 2015) has been set up to simulate ocean circulation and thermodynamics in the Iroise Sea. This model provides horizontal and vertical velocities as well as temperature and salinity distribution in a three-dimensional environment. The modeled area extends over the whole Iroise Sea, from 47.5 to 49.5° N and 4 to 6.5°W with horizontal resolution of 1.5 km and 30 sigma levels vertically. A single year is integrated three times by repeating the simulation with a set of forcing and boundaries conditions derived from observations made during the year 2007. Results discussed in this study cover a period of one month corresponding to September of the third year. This choice is justified by the fact that September is the period when the Ushant Front is most pronounced both in observations and in our simulations (see Fig. 9 in the companion paper Cadier et al., 2017). Expression of the processes shaping the diversity in this frontal environment is therefore most pronounced during this period. Moreover, this limited time period of one month also allows analysis of high frequency variability in the tidal front properties while avoiding bias in the zonal front position resulting from a longer integration period and that is not addressed by this study.

2.2. Biological and ecological model

The biogeochemical model that has been used in this study is derived from the DARWIN model (a general description of this model and equations is found in Follows et al., 2007). This model resolves lower trophic levels with the phytoplankton compartment divided into 120 phenotypes and the zooplankton compartment consisting of two size classes (micro- and mesozooplankton). It also simulates inorganic nutrients (nitrogen in different forms, phosphorus and silica) as well as dissolved and particulate organic matter. Phytoplankton phenotypes are equally divided into four functional types. Among them, two are small and belong to the picoplankton size class with a low maximum growth rate but high affinity for nutrients ('K' strategy). They loosely represent either *Prochlorococcus* sp. analogs (PRO) that use only ammonium as a source of nitrogen for growth or *Synecococcus* sp. and more generally picoeucaryote analogs, labeled as the 'small non *Prochlorococcus*' (SNP) generic group. The two other phytoplankton groups represent large, microphytoplankton cells with conversely higher growth rate ('r' strategy) but lower affinity for nutrients and light compared to small cells. Some within this category require silica to grow and are assigned to diatoms (DIA) while the remaining phenotypes are called 'Large Non Diatoms' (LND), comprising mainly dinoflagellates and nanoflagellates with lower maximal growth rates than diatoms.

A trade-off between growth rate and nutrient affinity is therefore considered (Grover, 1991) with a differential uptake strategy (see appendix A) between large, fast-growing opportunistic phenotypes having high nutrient requirements and small ones, with low maximum growth rate and relatively low half-saturation constants (Litchman et al., 2007). Moreover, large phytoplankton needs higher light intensity to grow whereas small-size cells are likely to grow under lower light levels (Edwards et al., 2015). Each phenotype is also given a specific temperature optimum for growth, which is not constrained by the size.

Indeed, within the four functional groups (with 30 phenotypes per group), each phytoplankton phenotype is unique, with its own particular combination of growth parameters associated with temperature, light intensity and nutrient requirements, randomly assigned from a plausible range of parameters defined by the functional group. This random selection of parameters results in a large mixture of phenotypes each of which has optimal growth potential in fairly unique environmental conditions.

Phytoplankton specific growth rate (for phenotype noted *j*) per unit of time can thus be written as:

$$\mu_j = \mu_{max,j} \cdot \gamma_{NUT,j} \cdot \gamma_{T,j} \cdot \gamma_{I,j} \cdot P_j.$$

With μ_{max} the maximum growth rate (day^{-1}), $\gamma_{NUT,j}$, γ_T and γ_I the growth limitations by nutrients, temperature and light, respectively, and P$_j$ the concentration of phenotype *j* (mmolC·m^{-3}). The detailed parameterizations for phytoplankton growth limitation are given in appendix A.

Phytoplankton phenotypes are also grazed by the two-zooplankton size classes, following diet preferences established on predator/prey size ratio rules. The prey selectivity is parameterized using an active prey switching ('kill-the-winner') formulation (Vallina et al., 2014b) in which an increased predation risk is assigned to the most abundant and therefore most accessible and profitable prey, thus enhancing coexistence among phytoplankton types and stability in ecosystem dynamics (Kiørboe et al., 1996; Gentleman et al., 2003). An additional phytoplankton natural loss term is also added for each phenotype and sinking occurs for large cells only.

Specific parameters' values that are used in the simulation are described in details in Cadier et al. (2017).

Our model setup allows the emergence of entirely new phytoplankton phenotypes through substitutions of unadapted ones while a simulation is underway. A phenotype experiencing no positive growth anywhere in the model grid suffers only biomass reductions; when its biomass falls below 10^{-6} mmolP·m^{-3} in all grid cells, it is removed from the system and replaced by a new, randomly assigned, homologous phenotype from the same functional group. Newly created phenotypes are homogeneously initialized at 10^{-4} mmolP·m^{-3} throughout the model domain and are assigned a unique phenotype number (thus exceeding 120 as soon as a first substitution occurs). This method allows each phenotype, corresponding to a unique and specific combination of growth parameters, to be easily tracked in time and space.

The number of substitutions decreases over time, with a plateau achieved after the first year and some convergence toward fewest substitutions during the third year (Fig. 2, A and C). The community tends to optimize with respect to regional environmental conditions with some regionally adapted phenotypes being maintained throughout winter from one year to the next although the substitution rate remains highest during winter. Indeed, the frequency of substitutions in all groups decreases during summer (Fig. 2) as environmental conditions (mainly temperature and, to a lesser extent, light availability) become more favorable to growth.

The use of substitutions during simulations allows a considerable reduction in the number of simulations by testing numerous growth strategies simultaneously while using a limited number of phytoplankton variables. The same effect has been demonstrated by Sauterey et al. (2014) using periodically generated mutations within the phytoplankton community and resulting in an increase in robustness of modeled patterns and enhanced repeatability among runs with low initial richness. Therefore, this method allows a better sampling of traits space within the phytoplankton community and leads to faster convergence toward an 'optimal' community at the regional scale compared to the classical 'everything is everywhere' (EIE) approach with fixed phytoplankton strategies (Follows et al., 2007; Dutkiewicz et al., 2009), although long-term emergent ecosystem properties remain unchanged.
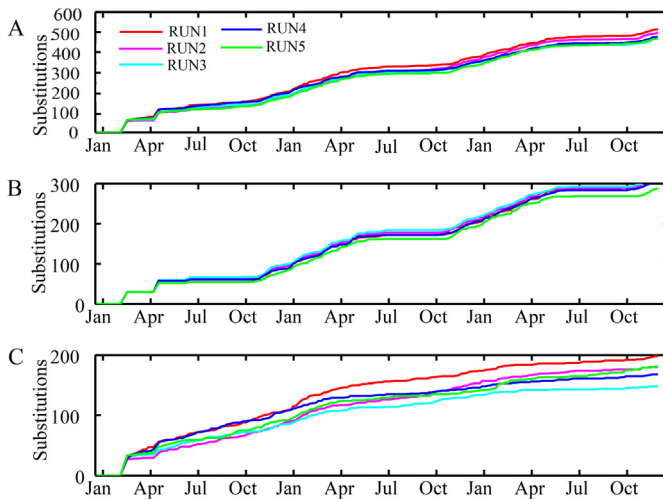
Fig. 2. Three year cumulative sums of the number of substitutions inside (A) total phytoplankton population, (B) *Prochlorococcus* sp. group only and (C) total phytoplankton except *Prochlorococcus* sp. analogs for five different realizations of the simulation.

As a consequence, we based our work on the study of five realizations of the simulation with different initial seeding (different random collections of growth rate parameters). In those simulations, an average of 182.4 substitutions occurs during the first year, and 166.6 and 137.2 occur for second and third years, respectively. Moreover, all five realizations lead to similar results in terms of temporal dynamics of substitutions during the three simulated years (Fig. 2). Prognostic selection of communities' average functional traits according to environmental conditions in light, temperature and availability of macronutrients is also quite similar across realizations (Fig. 3). Due to those similarities and for brevity, the subsequent presented results are based on only one of the five realizations. Careful attention has been given to the universality

(among our five realizations) of the processes highlighted in the chosen realization.

Prochlorococcus sp. analogs are the most frequently substituted phenotypes with 113 substitutions during the third year of the selected simulation; these mainly occur during the winter period due to their high temperature optimum that makes them poorly suited to modeled wintertime temperatures generally below 15 °C. The group with the minimal number of substitutions is the SNP group with 7 substitutions, while LND and DIA go through 9 and 13 substitutions during the third year, respectively. The September, monthly average number of substitutions is 3.4 over the three years (1.7 in DIA, 0.7 in LND, 1 in SNP and no substitutions in PRO), indicating that the proportion of substituted phenotypes is not likely to interfere with our results in terms of diversity in a significant way.

2.3. Diversity measurements

2.3.1. Local diversity α

We measure the modeled species richness S in each grid point as the number of phenotypes j whose concentration P_j exceeds a relative threshold of 1% of total biomass P_{tot}.

$$S = \sum_{j=1}^{N} \left(P_j > \frac{1}{100} P_{tot} \right)$$

A phenotype resulting from substitution is added to the system at very low biomass throughout the domain and thus does not contribute to the calculation of species richness in any grid cell unless it has undergone an increase in its local concentration such that it contributes to at least 1% of total phytoplankton biomass in that cell. This approach prevents an artificial species richness count due to substituted phenotypes in low phytoplankton biomass regions.
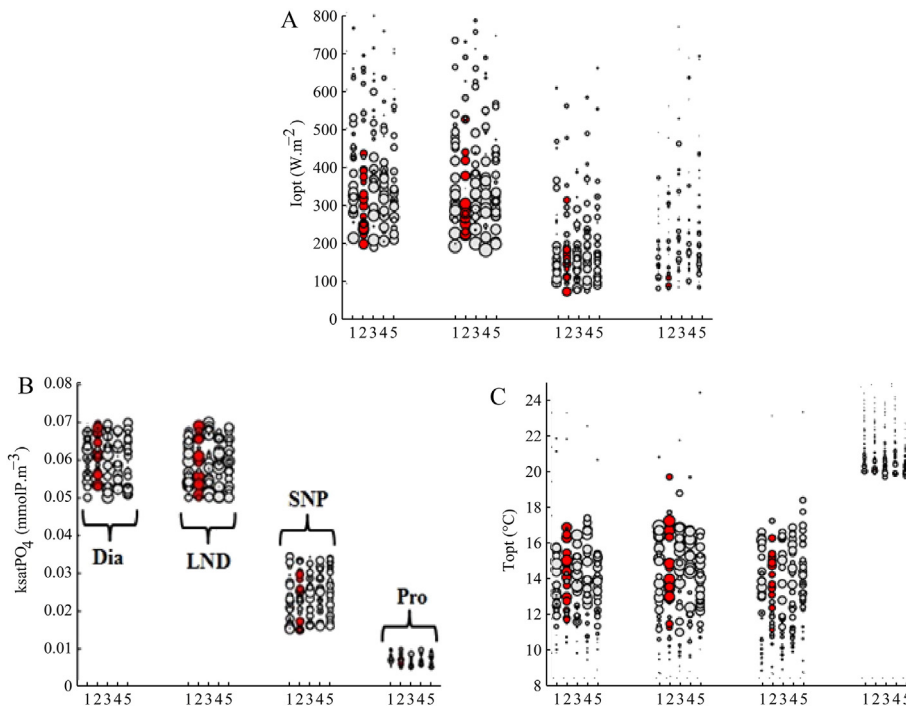

Fig. 3. Realized trait space in September for (A) light optimum (W·m^{-2}), (B) phosphorus half saturation constant (mmolP·m^{-3}) and (C) temperature optimum (°C) inside each functional group; from left to right: diatoms, Large Non Diatoms (LND), Small Non Prochlorococcus (SNP) and *Prochlorococcus* sp. analogs for five realizations of the simulation. Scatter size is proportional to the monthly average relative biomasses of each phenotype over the mixed layer during September. The second realization is used for subsequent analyzes. Ubiauitous phenotypes are represented in red.

2.3.2. Evenness index

Because rare and abundant phenotypes are counted equally in the species richness S, we use the Shannon-Wiener index H to better quantify equitability between phenotypes in each location of our model. This complementary index provides an 'evenness' measure of richness by accounting for both the number of coexisting phenotypes and their relative proportion (P_j/P_{tot}). We compute exp. (H) to get an effective number of phenotypes that helps the interpretation of the index (Jost, 2006).

$$\exp(H) = \exp\left(-\sum_{j=1}^{N}\left(\frac{P_j}{P_{tot}}\ \ln\frac{P_j}{P_{tot}}\right)\right)$$

3. Results

3.1. Model solution

3.1.1. Functional traits selection

Each phytoplankton phenotype exhibits a distinct combination of growth parameters concerning its preferences for light, temperature and nutrients. Monthly mean traits are thus calculated and provide insight into successful parameters in different regions (Fig. 3). Indeed, realized phytoplankton communities within simulations consist of phenotypes that, based on their growth parameters, are better adapted to modeled environmental conditions.

In particular, strong selection pressure occurs due to light affinity in September. Overall, regardless of the functional group or the region considered, phenotypes that have the highest affinity for low light levels are preferentially selected (Fig. 3, A). For microphytoplankton (i.e. DIA and LND), the most abundant phenotypes in terms of monthly average biomass display light optima between 200 and 400 $W \cdot m^{-2}$. Within picoplankton (i.e. SNP and PRO), phenotypes that grow optimally between 100 and 200 $W \cdot m^{-2}$ are the most competitive. *Prochlorococcus* sp. analogs are prescribed to require higher temperature for growth compared to the rest of the simulated phytoplankton community (Cadier et al., 2017). Consequently, temperature optima are even more discriminating than light optima for this group (Fig. 3, C), and phenotypes that predominantly contribute in significant proportion to biomass have temperature optima below 22 °C. Among other groups (DIA, SNP and LND), growth is promoted for phenotypes which have temperature optima in a less discriminant range, generally between 12 and 18 °C. Finally, differences in nutrient affinity do not act as strong discriminating factors for selection within functional groups (Fig. 3, B). In a given functional group (i.e., DIA, LND, SNP and PRO), the growth of the different phenotypes only weakly depends on their nutrient half-saturation constants, and they are quite distributed over the entire range of biomass irrespective of this parameter. However, nutrient affinity does explain most of the inter-group variability, since large phenotypes have higher nutrient requirements than smaller ones. The nutrient distribution is thus responsible for phytoplankton community bioregionalization in terms of functional groups in summer (Cadier et al., 2017).

3.1.2. Surface distribution

During summer, the tidal front separates tidally mixed waters over the continental shelf from stratified waters offshore. The surface mixed layer does not exceed a monthly average of 15 m depth in the deepest offshore region while the shallower continental shelf waters are regularly homogenized by tides over the entire water column. Indeed, the averaged surface mixed layer depth is deeper in the North East region and reaches the bottom boundary layer near the coast, with less light available for photosynthesis (Fig. 4, A). On average in September, the domain is thus characterized by a horizontal temperature gradient at the surface with colder temperatures around 13–14 °C in the well-mixed region compared to warmer temperatures of 17–18 °C

in the south-west (Fig. 4, C). The distribution of phytoplankton phenotypes reflects these environmental conditions, with the community having higher average temperature optima (16–17 °C) in the offshore surface layer (Fig. 5, C). *Prochlorococcus* sp. analogs represent ~40% of the total phytoplankton biomass in this region (Fig. 4, F).

Fig. 5 B shows higher phosphate half saturation constants (0.05–0.06 $mmolP \cdot m^{-3}$) within coastal, well-mixed waters compared to surface waters of the seasonally stratified South-West region (~0.03 $mmolP \cdot m^{-3}$). The coastal tidally-mixed region is dominated by microplanktonic cells (i.e. LND and DIA), with three times greater concentration than picoplankton cells (SNP and PRO). In contrast, surface waters of the stratified west side of the front are more suitable for picoplanktonic cells that coexist with larger ones or dominate in the shallow surface mixed layer (Fig. 4, E). This behavior is directly constrained by higher nutrient concentrations in the well-mixed waters east of the front (exceeding 0.3 $mmolP \cdot m^3$) compared to those in offshore, oligotrophic surface waters (Fig. 4, B).

The frontal region itself does not provide local specific ecological characteristics in terms of phytoplankton functional group distribution (Cadier et al., 2017) or realized functional traits (Fig. 5) although it exhibits the strongest simulated phytoplankton biomass, reaching >200 $mgC \cdot m^{-3}$ in September (Figs. 4, D and 6, A).

With regard to realized light traits, higher light requirements are simulated in the well-mixed coastal waters (Fig. 5, A) with averaged values for light optima of ~260 $W \cdot m^{-2}$. Conversely, offshore surface waters contain phenotypes with higher affinity for low light levels despite this region having the highest mixed layer average photosynthetic available radiation in the model domain (Fig. 4, A). Indeed, in the stratified region, phytoplankton optimal growth is reached for a light intensity of ~200 $W \cdot m^{-2}$. The presence of fewer phenotypes adapted to low light conditions in the less illuminated waters of the well-mixed region is connected to the trade-off between functional groups, foremost selected through their differential affinity for nutrients. Indeed, picoplankton cells (i.e., SNP and PRO), which predominate in the oligotrophic, highly illuminated surface waters to the west, are characterized by both low half saturation constants for nutrients and low light requirements.

3.1.3. Vertical structure

The vertical structure of phytoplankton biomass along the 48°N transect (Fig. 6, A) reveals high concentrations of 200 $mgC \cdot m^{-3}$ between 0 and 20 m at the physical position of the front where isopycnal intersect the surface. The stratified region west of the front displays a deep chlorophyll maximum (hereafter DCM) at about 30 m depth on average in September, with biomass of ~100 $mgC \cdot m^{-3}$, about half that of the frontal maximum value. In this stratified region, the community composition in terms of realized mean traits does not show a significant change in the light optima between the surface and DCM depth (Fig. 6, B). Indeed, only the distributions of communities' realized traits associated with temperature and nutrient affinities are vertically structured in stratified waters (Fig, 6, C and D). Hence, the surface mixed layer provides optimal growing conditions for *Prochlorococcus sp.*, consequently leading to a community having higher temperature optima, exceeding 16 °C (Fig. 6, D), and very low phosphate half saturation constants, below 0.04 $mmolP.m^{-3}$ (Fig.6, C). In contrast, SNP, that have slightly higher requirements in nutrients concentrations compared to *Prochlorococcus* sp. analogs, are rather dominant at the DCM depth (Cadier et al., 2017) which exhibit a biomass-weighted half saturation constant between 0.045 and 0.05 $mmolP \cdot m^{-3}$ and a community temperature optimum below 15 °C.

3.2. Modeled diversity

The surface α diversity (S) is computed over the surface mixed layer for each day of September and time averaged. The largest richness of
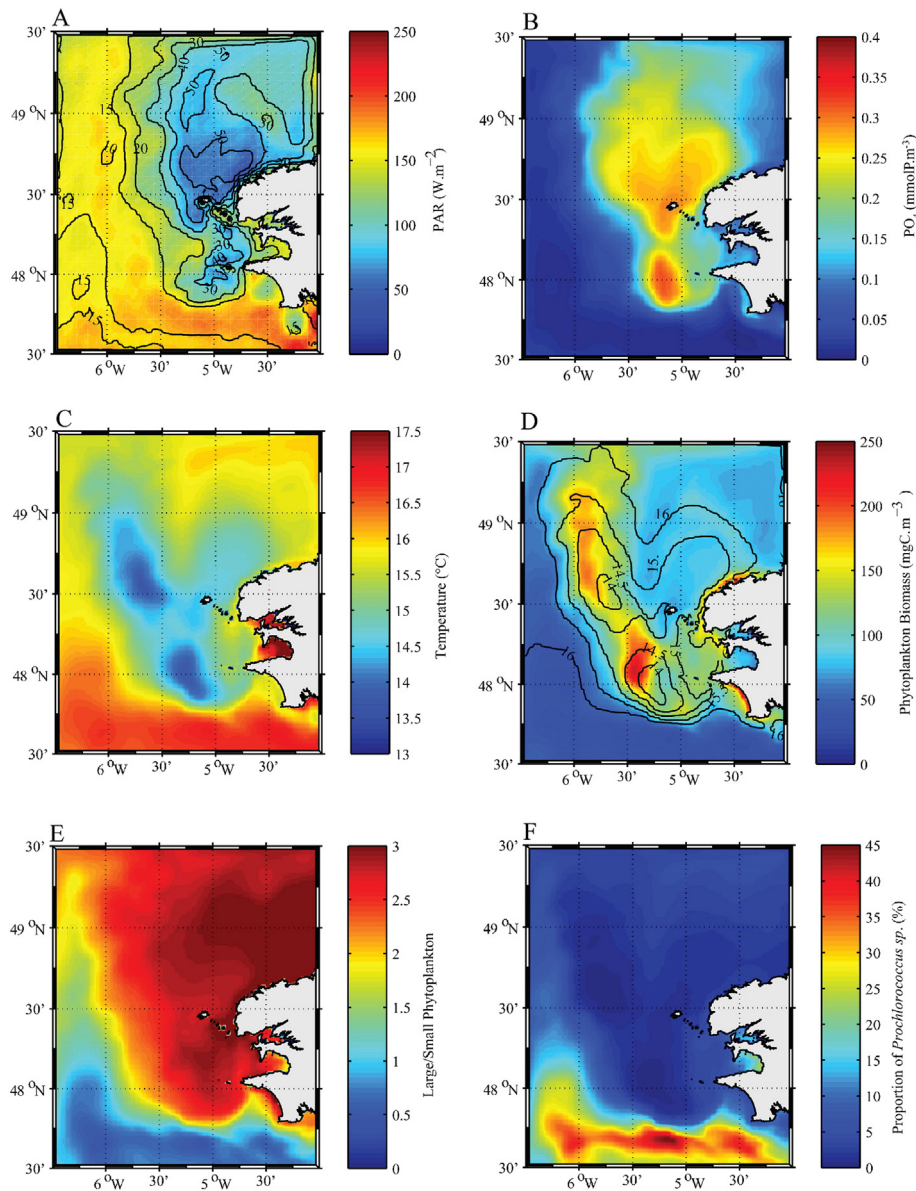
Fig. 4. Monthly (September) average, over the surface mixed layer, of (A) photosynthetic available radiation (W·m^{-2}) with contours of surface mixed layer depth (black line), (B) phosphate concentration (mmolP·m^{-3}) with the 48°N longitudinal transect (red line), (C) temperature (°C), (D) phytoplankton biomass (mgC·m^{-3}) with contour of temperature (black line), (E) large/small phytoplankton ratio and (F) proportion of *Prochlorococcus* sp. phenotypes over total phytoplankton biomass. (For interpretation of the references to color in this figure legend, the reader is referred to the web version of this article.)

~45–48 coexisting phenotypes is located slightly west of the maximum biomass at the Ushant Front (Figs. 7, A and 4, D). The map of exp.(H) shown on Fig. 7, B follows a similar spatial distribution to richness with a maximum of 70 phenotypes immediately west of the front position; thus that the phenotypic richness increase in the area immediately west of the front location is associated with both the presence of a large number of phenotypes and a large degree of evenness in their concentrations. In addition to this maximum at the surface, the vertical structure of time-average local phenotypic richness (i.e., α diversity) shows an intermediate diversity level of ~42 phenotypes in the DCM (Fig.7, C) and at the Ushant Front slightly east of the surface maximum and extending over the whole water column. The tidally well-mixed region near the coast and offshore surface oligotrophic waters host lower richness with ~40 phenotypes exceeding 1% of the total biomass. The Shannon Index (exp(H)) reveals a quite similar vertical distribution (Fig. 7, D) when compared to the α diversity despite values in the stratified waters approximating those of the surface diversity maximum (Fig. 7, C).

Furthermore, the contributions of the four functional groups to the total diversity (Fig. 8) display very different patterns. The diatom diversity presents lower spatial variability than other groups and is maximal in the tidally mixed region of our modeled domain. Conversely, the diversity of LND and SNP groups exhibit highest values coinciding with the larger total diversity, west of the Ushant Front. *Prochlorococcus* sp. is represented by a significantly smaller number of phenotypes mostly simulated in the surface oligotrophic warm waters of the stratified region.

3.3. Community composition of the diversity maximum

In this section, we seek to describe and understand the composition of the high local diversity simulated in the surface mixed layer, slightly west of the front compared to nearby regions: is there a mix of phenotypes from surrounding populations or local growth of very specific phenotypes?
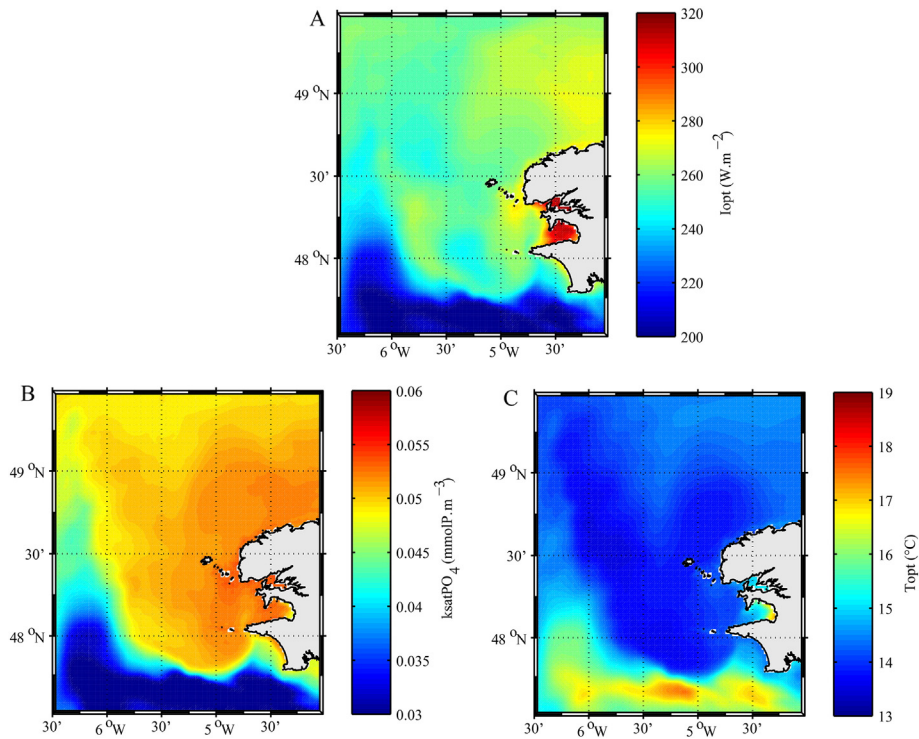
Fig. 5. Monthly average of mean values of functional traits weighted by phytoplankton biomass in the surface mixed layer in September: (A) light optimum ($W \cdot m^{-2}$), (B) phosphorus half saturation constant ($mmolP \cdot m^{-3}$) and (C) temperature optimum (°C).

To tackle this issue, the study area was separated into four time-varying sub-regions in order to capture differences or similarities between the diversity maximum and adjacent hydrographic regimes (Fig. 9, A). The grid points in which computed diversity in the surface mixed layer is between 80% and 100% of the simulated spatial maximum of local α diversity defined the (i) diversity maximum cluster (hereafter denoted as DM). Among remaining grid points, a stratified sub-region is defined by the presence of a subsurface chlorophyll maximum. This latter is then vertically separated into distinct (ii) surface

oligotrophic layer (called SSW for Surface Stratified Waters) and (iii) DCM depth at which phytoplankton biomass is maximal. Finally, the (iv) eastside well-mixed sub-region consists of vertically homogeneous locations in which the vertical density gradient ($\Delta\rho/\Delta z = (\rho_{bottom} - \rho_{surf}) / h$ where ρ is the density and h the depth of the water column) does not exceed a threshold value of $0.008 \, kg \cdot m^{-4}$. This last sub-region is called MW for Mixed Waters.

Differences between sub-regions, based on relative phenotype concentration and distribution have been tested by the nonparametric
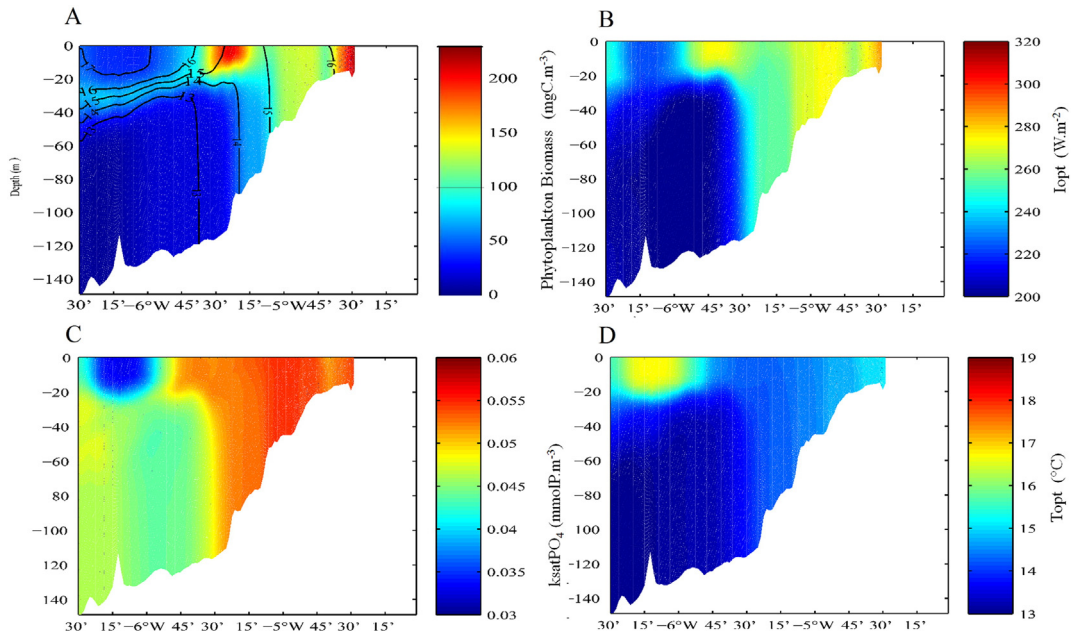

Fig. 6. Vertical distribution of (A) total modeled phytoplankton biomass ($mgC \cdot m^{-3}$) along the 48°N transect (Fig. 4, B) with the surface isotherms (°C). Vertical structure of September monthly average of functional traits weighted by phytoplankton biomass: (B) light optimum ($W \cdot m^{-2}$), (C) phosphorus half saturation constant ($mmolP \cdot m^{-3}$) and (D) temperature optimum (°C).
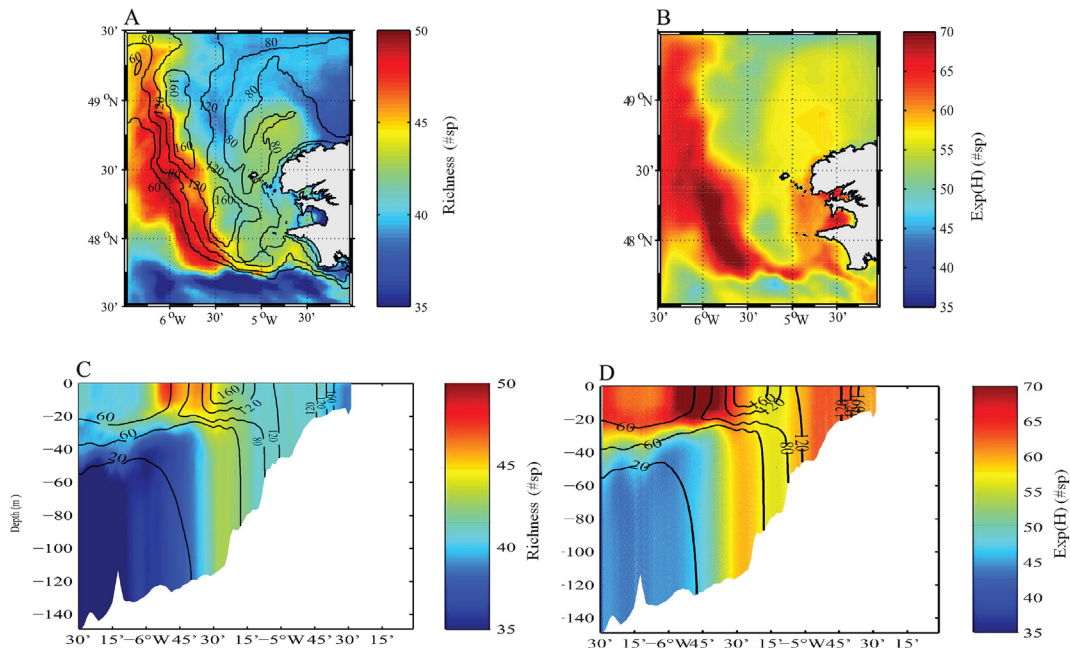
Fig. 7. Monthly september average of (A, C) phenotypic diversity (α richness) and (B, D) Shannon – Wiener Index exp.(H) over the surface mixed layer (A, B) and along the 48°N transect (C, D). Black contour lines on (A), (C) and (D) indicate phytoplankton biomass (mgC·m^{-3}).

Wilcoxon ranksum test (Gibbons and Chakraborti, 2011) on pairs of samples originating from (i) the diversity maximum and, alternately (ii) each of the three others sub-regions (Table 1). The number of common species between (i) and (ii) is also listed in Table 1. We refer to phenotypes as present within a location (and thus in a particular

hydrographic regime) if their concentration contributes to >1% total phytoplankton biomass (i.e., contributing to our local diversity calculation).

The test reveals no significant difference in the community composition between the DM, the diversity maximum and MW (Table 1,
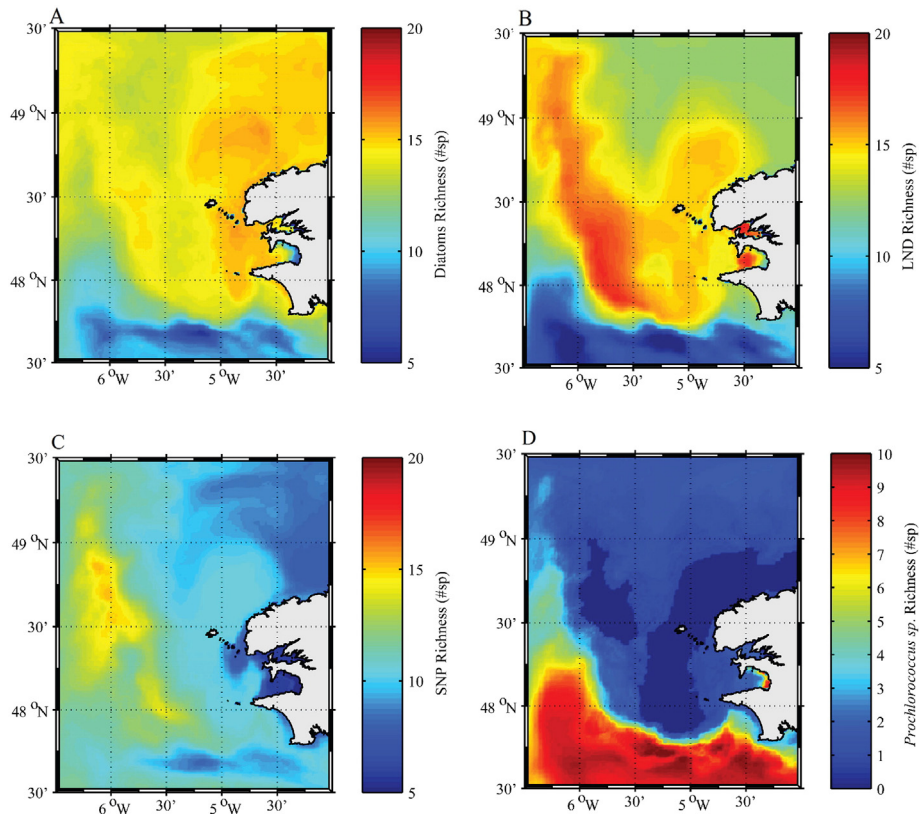

Fig. 8. September monthly average phenotypic richness (α) belonging to (A) diatoms, (B) LND, (C) SNP and (D) *Prochlorococcus* sp. analogs groups over the surface mixed layer. Richness is expressed as the number of phenotypes contributing >1% to total biomass in each functional group. Note that different scale is used in (D).
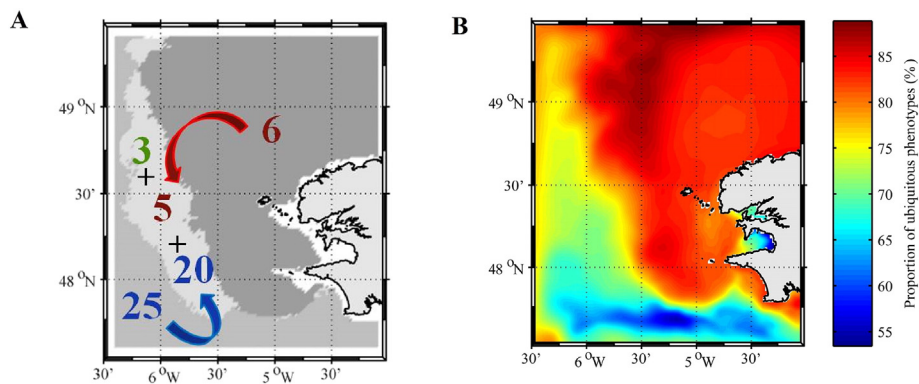
Fig. 9. (A) Number of non ubiquitous phenotypes in coastal well-mixed waters (red) and in stratified offshore waters (blue) and number of non-ubiquitous phenotypes in diversity maximum shared with coastal mixed waters (red), shared with stratified offshore waters (blue) and specific to diversity maximum (yellow). (B) Time averaged percentage of total phytoplankton biomass (mgC·m^{-3}) represented by ubiquitous phenotypes in the surface mixed layer.

p-value = 0.56) and between the DM and DCM on the stratified west side (p-value = 0.93). The phytoplankton community simulated at the diversity maximum is thus close to that of the coastal well-mixed waters and the DCM in terms of relative proportions of the different phenotypes. On the contrary, the SSW exhibits significant differences in their phenotypes' relative distribution (p-value = 2e-5); this result suggests that different environmental pressures and traits influence selection.

However, the community simulated in the SSW shares the highest proportion of 63 phenotypes with that in the diversity maximum (including 20 non ubiquitous; Fig. 9, A) (Table 1). The same phenotypes are present in both regions but their relative distribution varies significantly, which should be related to differences in local environmental conditions and phenotype fitness.

The regional diversity (γ diversity) is defined as the total number of phenotypes accounting for the local diversity α at least once at any location of our four sub-regions and at any time within the considered period. Thus, in September, simulated γ diversity is 77 phenotypes. Among them, 48 are ubiquitous (i.e. counted in diversity of all sub-regions). Excepting six phenotypes (Fig. 9, A), the MW sub-region contains mostly ubiquitous phenotypes that accounted for ~80% of the total biomass (Fig. 9 B and 10). MW and DM have 53 phenotypes in common (Table. 1) including only 5 non-ubiquitous (Figs. 9 A and 10). Almost every phenotype within MW (all except one) is present in similar relative proportion within the diversity maximum (Table 1, Wilcoxon test).

Table 1
Total number of phenotypes in the diversity maximum (2nd column) and number of shared phenotypes between diversity maximum and each of the three areas between diversity maximum and each of the three sub-regions (3rd to 5th columns) of (i) well mixed coastal waters, (ii) stratified surface waters and (iii) DCM waters for the total phytoplankton, diatoms only, LND only, SNP only and Prochlorococcus sp. (PRO) analogs only.
p-Value of the sum-rank Wilcoxon test of the phenotypic community composition between diversity maximum and each of the three sub-regions. Asterisk indicates that the difference is not statistically significant at the 5% level.

	Diversity maximum	Coastal mixed water	Stratified surface waters	Stratified-DCM
	Richness	Number of shared phenotypes with diversity maximum		
Total phytoplankton	71	53	63	60
DIA	18	17	17	17
LND	21	18	18	17
SNP	21	16	18	18
PRO	10	2	10	8
	Wilcoxon test result			
p-Value over diversity maximum		0.56*	2e-5	0.93*

In addition to those 53 phenotypes shared with the MW, DM contains specific phenotypes from the south-western stratified waters from both the SSW (15 phenotypes) and DCM (12 phenotypes) (Table 1 and Fig. 10, A, C and D). These extra phenotypes, that are not represented in the MW are almost all characterized as picophytoplankton (i.e., SNP or PRO) (Table 1; Fig. 10). Indeed, microphytoplankton (i.e., DIA and LND) is much more ubiquitous (Fig. 11) with the same number of phenotypes shared between the DM and each of the three other regions (Fig. 8; Table 1) compared to picoplankton that shows higher diversity in the SSW (PRO) and MD (SNP) (Fig. 8, C and D) than in the MW.

The stratified region contains more specific non-ubiquitous phenotypes (25) compared to well-mixed coastal waters (5) (Fig. 9, A). Those specific phenotypes account for ~50% of the total carbon biomass (Fig. 9, B).

Specific picoplanktonic phenotypes from the stratified region and present in the DM grow either in the SSW and/or at the DCM depth (Fig. 10). Thus, all PRO phenotypes counted in diversity of the DM grow in the SSW and DM. Some of these phenotypes are also present within the DCM, but they generally do not show a positive local net growth as they do at the surface (Fig. 10, C). The only exception that grows within the DCM is PRO570 (Fig. 10, D). It has the lowest light optimum among the Prochlorococcus sp. group and is thus more optimized for deeper waters (Fig. 11). PRO phenotypes that are present within DCM are overall those with low light optima and low temperature optima compared to other non ubiquitous PRO (Fig. 11).

Unlike Prochlorococcus sp., SNP that contribute to the DM phytoplankton pool come from either the DCM or SSW and are vertically segregated. Half of these SNP phenotypes experienced positive net growth within the DCM (Fig. 10, D) whereas others have significantly higher light and temperature optima (above 200 W·m^{-2} and 12·5 °C) and are present only in the SSW on the stratified side (although they do not exhibit positive net growth) (Figs.10, C and 11). Interestingly, some SNP phenotypes growing at the DCM are absent from the DM (Fig. 10, D) because of their low temperature optima (below 12 °C; Fig. 11).

Nonetheless, all SNP phenotypes shared between stratified waters to the south and west of the domain and the diversity maximum just west of the front (including those growing within the DCM) do not exhibit local growth in the diversity maximum. These results suggest physical transport between these two locations (Fig. 10, A and D).

The diversity maximum is thus a mix between ubiquitous phenotypes and specific phenotypes from both the MW and to a larger extent the stratified waters. In addition, among non ubiquitous phenotypes, only six are present at the regional scale, in either the SSW (1), DCM (4) and/or MW (1) while being absent in the DM and three phenotypes are exclusively present in the DM (Fig. 9, A). Those specific phenotypes are from the LND functional group and have positive net growth within the diversity maximum (Fig. 10). Their presence, probably enabled by
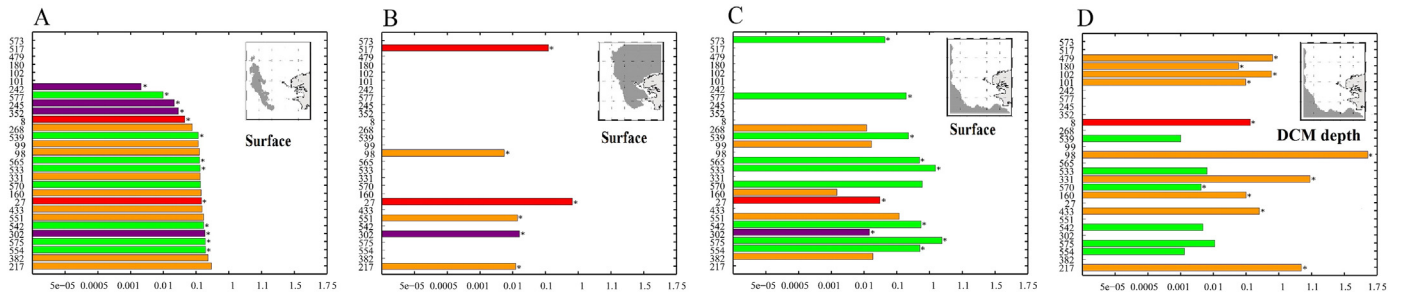
Fig. 10. Compared biomass of non ubiquitous phenotypes for (A) diversity maximum, (B) coastal well-mixed waters, (C) surface stratified offshore waters and (D) Deep Chlorophyll Maximum (DCM) of the stratified side in September. Diatoms: red; LND: purple; SNP: orange and *Prochlorococcus* sp.: green. (For interpretation of the references to color in this figure legend, the reader is referred to the web version of this article.)

the high light optima (Fig. 11) could explain the higher LND proportion in total diversity in the DM (Fig. 8).

3.4. Distribution of locally adapted vs. exported phenotypes

To quantify the relative role of biological growth and physical transport in the simulated phytoplankton diversity patterns, we estimate local net growth for each phenotype j. This term μ_j^{NET} (mmolC.m^{-3}.-day^{-1}) represents the net balance between the phenotype's gains (μ_j) and losses (linear mortality through cell lysis and pathogens (m_j) and predation by grazers ($graz_j$)) as a function of local environmental conditions only (i.e., not affected physical processes of advection or mixing).

$$\mu_j^{net} = \left(\mu_j - graz_j - m_j\right) \cdot P_j$$

A positive μ_j^{NET} indicates that phenotype j is well adapted to local environmental conditions, including both abiotic influences (e.g., resources, temperature) and biotic factors (competitors and grazers), and is able to increase its concentration and contribute to local diversity. Conversely, a phenotype that contributes to local diversity but does not show a positive net growth ($\mu_j^{NET} < 0$) is either maintained by a source due to physical transport (i.e., neutral theory) or in decline.

Indeed, the temporal change of phenotype j, $\frac{dP_j}{dt}$ in each grid point is constituted by both biological processes (μ_j^{NET}) and physical terms of advection/mixing written as M_j (mean transport) and V_j (vertical mixing):

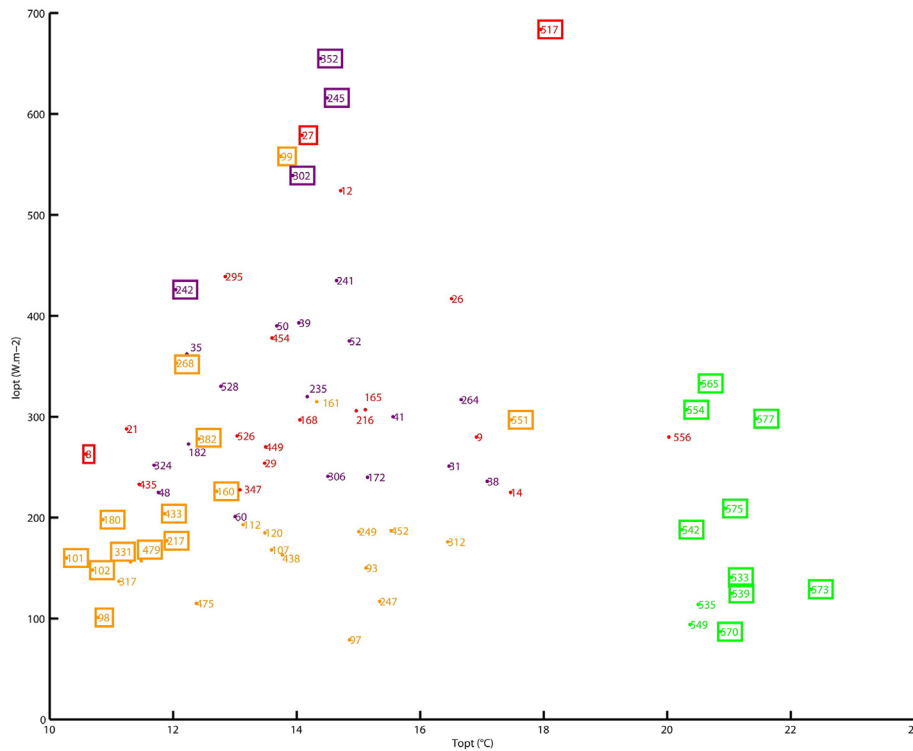$$\frac{dP_j}{dt} = \mu_j^{net} + (M_j + V_j) \cdot P_j.$$

Fig. 11. Trait space of light and temperature optima for regional phenotypes pool of (i) diversity maximum, (ii) coastal well-mixed waters, (iii) surface stratified offshore waters and (iv) Deep Chlorophyll Maximum (DCM) of the stratified side. Diatoms: red, LND: purple, SNP: orange and Prochlorococcus sp.: green. Non ubiquitous phenotypes (total of 29) are represented in boxes of different shape. For SNP and PRO: ▭ shared between DCM and Diversity Maximum; △ shared between surface stratified waters and Diversity Maximum; ◇ found only on stratified side (DCM for SNP and surface for PRO) and ◇ shared between Diversity Maximum, DCM and surface of stratified waters (full line: growing only at surface; dotted line: growing only at DCM depth). For LND: △ found only in Diversity Maximum and ▭ shared between Diversity Maximum, coastal well-mixed waters and DCM. (For interpretation of the references to color in this figure legend, the reader is referred to the web version of this article.)

Both biological rates (net growth without taking into consideration physical movement, Fig. 12, A and C) and physical transport ($M_j + V_j$; Fig. 12, B and D), including horizontal and vertical advection by currents, vertical mixing and diffusion, can be either positive or negative. To compute the contribution signs of those biological and physical transport terms, we compare, for each phenotype j, the effective temporal change in the phytoplankton concentration to its change expected in the absence of any motion. The resulting difference is either positive, indicating a biomass input from elsewhere through dynamical transport or negative, corresponding to net export of biological material.

The well-mixed region north east of the front is shown to be a local source of phytoplankton diversity where all phenotypes forming the total local α diversity (~43 phenotypes) have positive local net growth over the whole water column (Fig. 12, A and C). Moreover, lower effective rates of change in phytoplankton biomass than expected without any physical transport (Fig. 12, B and D) show that those phenotypes are exported from the north east part of the modeled domain.

In the stratified south west part of the Iroise Sea, positive local growth and physically-driven export happen within the DCM (Figs. 12, C, D and 13). In contrast, in the oligotrophic surface waters, about half of the phenotypes accounted in diversity exhibit positive local net growth (Figs. 12, A and 13 A). In addition, this region receives imported phenotypes through physical transport (Figs. 12, B and 13, B).

The phytoplankton biomass maximum at the front produces local diversity at the surface that is then exported from the surface layer (white box on Fig. 13) (13, A). Conversely, below this biomass maximum (>20 m depth), where light limitation due to self-shading occurs (Figs. 12, C and 13, A), diversity is rather imported than locally produced (Figs. 12, D and 13, B).

In contrast, slightly west of this front, the diversity maximum (green box on Fig. 13) is characterized by local growth at the depth of the DCM whereas the surface, where diversity is maximal, is filled with a majority of non autochtonous imported phenotypes (Figs. 12 and 13)

4. Discussion

Coastal regions are very heterogeneous environments in which physical and chemical properties display strong gradients and variability in the distribution of phytoplankton functional properties. In our simulations, the complex bathymetry and shallow continental shelf associated with strong tidal currents in the Iroise Sea lead to the existence of a summer bio-regionalization (as in observational data) with two contrasting regimes constituted by heterogeneously distributed phytoplankton biomass (Fig. 1). Higher phytoplankton biomass is simulated in the coastal, well-mixed and nutrient-replete region while offshore stratified, nutrient-depleted waters display lower biomass (Fig. 4, D). However, the most prominent feature of the simulated phytoplankton biomass is an observed (Fig. 1) and well documented (e.g., Pingree et al., 1978; Holligan, 1981; Le Boyer et al., 2009; Sun and Cho, 2010) maximum found within the Ushant front (Figs. 4D & 6A) that separates tidally-mixed waters from seasonally stratified oligotrophic waters during the summer period. Here, we have investigated whether the temporal and spatial variability of this complex environment influences the simulated phytoplankton diversity.

4.1. Global level phytoplankton diversity

Noticeably, simulated diversity in the Iroise Sea shows considerable homogeneity with relatively low spatial variability when compared to global diversity measures.

Indeed, the role of zooplankton, that grazes preferentially on most abundant phenotypes using an 'active-switching' formulation (Vallina et al., 2014b) reduces the contrast between different phytoplankton phenotypes distributions (Prowe et al., 2012). Following Chesson (2000), it tends to stabilize the community composition and increase simulated local diversity by decreasing the dominance of the most abundant phenotypes. Nonetheless, global scale diversity gradients
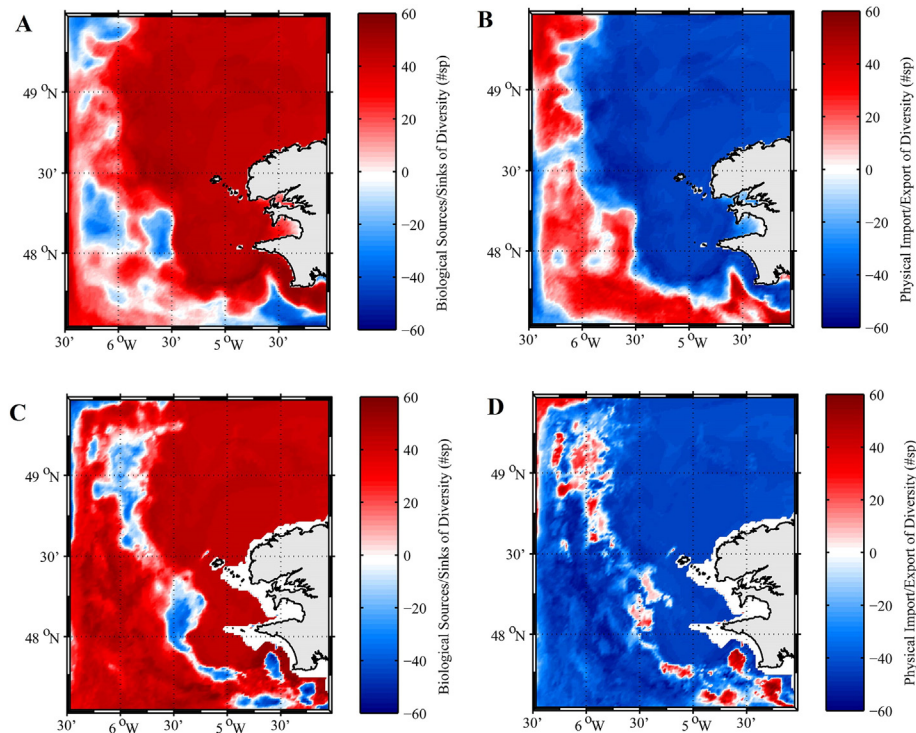

Fig. 12. (A–C) Spatial distribution of net difference between sources ($+$) and sinks ($-$) of phenotypic richness (expressed in number of phenotypes) due to biological processes (i.e. local net growth) for (A) the surface mixed layer and (C) the 30 m isobath (which corresponds to the Deep chlorophyll Maximum Depth). (B-D) Spatial distribution of imported ($+$)/exported ($-$) phenotypic richness due to physical transport for (B) the surface mixed layer and (D) the 30 m isobath. Represented value are computed as the difference between imported and exported phenotypes in each grid point. Black contour lines indicate phytoplankton biomass (mgC·m^{-3}) (A–C) and diversity (phenotypic richness) (B–C).
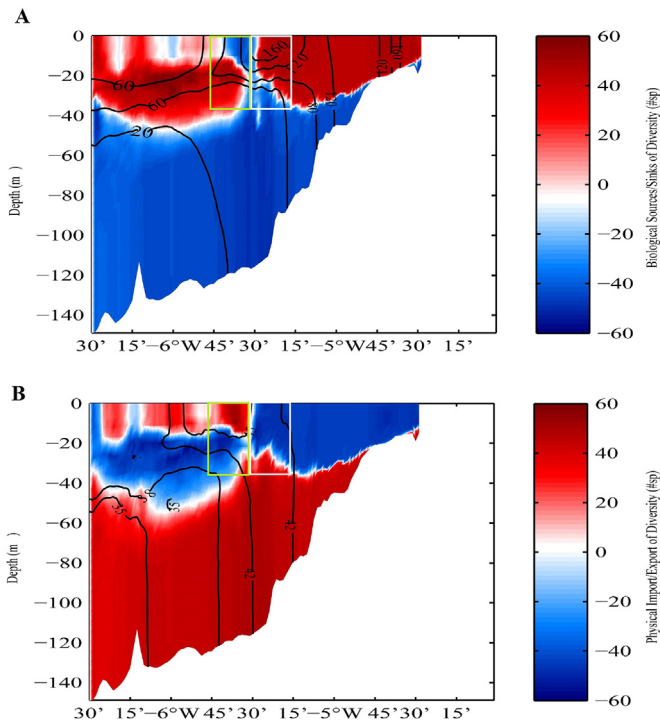
Fig. 13. Same as Fig. 12 but for the 48° N vertical section. (A) biological sources (+)/sinks (−) of phenotypic richness and (B) imported (+)/exported (−) phenotypic richness due to physical transport. Black line contours are (A) phytoplankton biomass (mgC·m^{-3}) and (B) phenotypic richness. White box encloses surface biomass maximum and green box encloses surface diversity maximum.

(Vallina et al., 2014a) are still higher than those simulated in our regional study, even if the same zooplankton parameterization is used. Regional variations simulated in the Iroise Sea reaches only about 10–15 phytoplankton phenotypes (varying between 35 and 50) while at global scale it is of the order of 50 phenotypes (when considering annual average of diversity).

A first obvious explanation comes from the geographical extent: although our domain encompasses two very different regimes (a nutrient-rich, productive zone and oligotrophic, stratified waters), the ranges of variation in parameters, mostly for light and temperature, are much smaller than those at a global scale (Vallina et al., 2014a). Moreover, at a global scale, the diversity gradient between very contrasted and remote regions cannot be overcome by physical transport of phenotypes, as can happen in smaller, contiguous regions like the Iroise Sea.

A second explanation is the substitution of non-surviving (i.e. non optimal) phenotypes during the simulation with new, randomly assigned phenotypes. This method forces the total number of phenotypes to remain stable (120 or 30 for each group) and to promote phenotypes with optimal fitness thus decreasing R* differences between phenotypes compared to sub-optimal communities. Nevertheless, although the diversity variability amounts to 10% of the total potential diversity, the five simulations undertaken with different initial random choices of traits show very similar behavior in the phytoplankton community structure, which gives us confidence in the robustness of our results.

4.2. Environmental selection of phytoplankton traits

On opposite sides of the frontal interface, the distribution of simulated phytoplankton functional traits is shown to be primarily driven by local nutrient concentrations that define the phytoplankton community regionalization. Microphytoplankton (consisting of DIA and LND) dominates in well-mixed, nutrient-rich waters (where biomass is almost

entirely constituted by ubiquitous phenotypes; Fig. 9, B). Nutrient concentrations are sufficiently high to create a non-nutrient limiting environment, and large cells, associated with high growth rates, become predominant in this turbulent environment. In contrast, in the surface oligotrophic waters of the stratified region, picophytoplankton (consisting of PRO and SNP) is more abundant (Fig. 4, E). In this region, phytoplankton experiences growth limitation (by nutrients at the surface and light at depth; see Figs. 4, A and 5). Phenotypes' success and simulated distributions of traits are thus driven by environmental selection pressure with specific phenotypes having the highest fitness and being locally advantaged. Indeed, in the stratified waters, almost half the total phytoplankton biomass is explained by a specific community (i.e., non ubiquitous; Fig. 9, B). Those phenotypes, mostly picoplankton (SNP and PRO), take advantage over microphytoplankton (DIA and LND) due to their growth limitation in stressed environments. The opposite scenario, exclusive competition in favor of large cells which prevents the efficient growth of picoplankton (as occurs in well-mixed coastal waters), does not happen in this offshore region.

There is no overlap between nutrient-affinity ranges (i.e., traits) of micro- and picophytoplankton (Fig. 3, B), leading to discrimination between the two groups according to nutrient conditions. The same holds for temperature: PRO can grow and survive mostly in the warmer oligotrophic surface waters. Conversely, the range of light optima overlaps between functional groups. Thus, light is not a discriminating factor between groups in our model results. This result is clearly visible in Fig. 6: in the stratified region, discriminating factors are either temperature or affinity for nutrients while light sensitivity traits are not vertically structured. Our model does not impose differences between the two groups of picophytoplankton (SNP and PRO) in term of light utilization through differential pigments composition. Thus, only the high temperature affinity of the PRO group (i.e., the PRO group is the fittest group in the warm surface layer) and the higher requirements for nutrients by SNP (i.e., SNP are the fittest at the DCM depth) drive the vertical distribution of these two groups (Cadier et al., 2017).

Contrasting with the selection process for functional groups (mainly driven by nutrients and temperature for PRO), the selection of phenotypes within the functional groups (i.e., at the intra-group level) is mainly driven by light (Fig. 3, A); applied ranges for nutrient half-saturation constants make all nutrient-affinity strategies viable within each functional group. For instance, SNP phenotype growth (i.e., intra-group level) is vertically distributed according to differential phenotypes' light optima (Fig. 11) in the two-layered stratified region.

Fig. 11 shows that the physiological characteristics of the ubiquitous phenotypes do not exhibit specific patterns, besides lying in the middle of the trait space. These ubiquitous phenotypes are widely distributed, and their fitness is not associated with extreme values of environmental factors. In contrast, (besides PRO which is mostly constrained by temperature), non-ubiquitous phenotypes show trait values which tend to be at the rim of the domain; they are associated with more extreme environmental parameters than ubiquitous phenotypes (e.g., local niches favor few phenotypes with high adapted fitness). Moreover, it seems that the traits of these non-ubiquitous phenotypes are globally correlated, with a tendency toward a parallel increase of T_{opt} and I_{opt} (not taking into account SNP551). This relationship is obviously linked to a correlation in the environmental parameters (e.g., temperature and PAR) and to the lack of explicit physiological trade-off in the choice of intra specific traits. This trait correlation or apparent "trade-off" mirrors the correlation between the physical parameters in the vertical dimension on the stratified side of the front (i.e., beneath the warmer and more lit surface layer). Without thus trade-off, the maximum fitness is obtained by optimizing independently each parameter (which tends to favor locally a small number of species), whereas physiological trade-offs prevent from optimizing fitness for each environmental parameter. This discussion shows a fundamental limitation of the model: the absence of intra group trade offs. Nevertheless, more knowledge on the physio-ecology of resource utilization by phytoplankton is needed in order to be able

to consider realistically these trade-offs. Keeping this drawback in mind, several important conclusions can nevertheless be drawn in terms of diversity (as done in all studies using DARWIN) and the coupling between frontal dynamics and phytoplankton diversity.

4.3. Relative roles of physical transport and biological growth in shaping diversity in frontal environment

In nature, the plankton distribution and its patchiness are regulated by both biological and physical processes that govern patterns of total plankton biomass and species composition (Legendre and Demers, 1984; Mackas et al., 1985). The major role of ocean dynamics (through both mixing and lateral stirring) in generating phytoplankton patchiness at fronts has been mentioned and investigated by countless field and theoretical studies (e.g. see the review by Martin, 2003).

If evolutionary processes are neglected because they are only meaningful on timescales longer than those addressed in this study, the responses of plankton assemblages have been shown to depend on the relative timescales of the biological and physical forcing (Abraham, 1998). Counteracting processes therefore affect both functional traits diversity and phenotypic richness. Competitive exclusion in a steady environment results in niche segregation and tends to decrease the diversity. In contrast, variability in physical and geochemical properties (temperature, irradiance and nutrient concentration) and passive transport by oceanic currents of allochtonous species will increase diversity.

In our study, we have distinguished two types of processes that are likely to affect phytoplankton diversity: local ecological (i.e. biological) processes and "migratory" passive fluxes (i.e., physical processes). Several distinct sub-regions have been identified in which one or the other kinds of processes are dominant to control the simulated phenotypes diversity. The coastal well-mixed waters, the highly productive frontal region (biomass maximum) and the DCM depth on the stratified side of the front are dominated by local phytoplankton growth whereas in surface waters of the stratified region (comprising the surface diversity maximum), passive transport prevails to explain the observed coexistence (Figs. 12 and 13).

Two main processes are proposed to explain the high species diversity in phytoplankton at fronts: (i) enhanced biological growth facilitated by nutrient supply from below the pycnocline (Legendre et al., 1986) to a relatively shallow, and therefore well lit, surface mixed layer (Franks, 1992) and (ii) physical mixing of different phytoplankton phenotypes adapted to different surrounding environments. In our case, the first process occurs mainly in the east part of front, corresponding to the biomass maximum in the presence of optimal growth conditions. However, in the western part of the frontal area and despite positive local growth for some phenotypes, the diversity maximum is rather sustained by advected phenotypes. Indeed, a mix of species from the eastern, tidally-mixed part of our domain and picoplanktonic phenotypes from the western stratified waters arises in the diversity maximum (located slightly west of the biomass maximum). Frontal dynamics that come from sharp density gradients at the front lead to large vertical motion in this region: the variance of the vertical velocity in September shows a maximum at the Ushant Front (Fig. 15, A). Upwelling vertical advection occurs to the west of the front where isotherms shallow to the surface (Fig. 14, B). Along with vertical mixing, this characteristic structure for oceanographic fronts (Yanagi et al., 1995) allows passive upward transport of phytoplankton growing within the DCM toward the surface west of the front, explaining the shift between the diversity maximum and the biomass maximum. Consistent with this result, the phenotypic composition of the diversity maximum is closer to the DCM composition than that from other regions (Table 1). The co-localization of different communities west of the physical front is thus mostly explained by hydrodynamics through front-induced upward advection of phytoplankton on the warm side of the front.

Phenotypes (SNP) that come from the DCM and are carried toward the surface do not grow locally in oligotrophic conditions but instead are imported exclusively through physical vertical exchanges (upward transport). Their presence in the diversity maximum suggests that they achieve sufficiently low R^* (measured taking into account transport terms; see Levy et al., 2014) to be maintained in significant proportions in the local phytoplankton community. The survival of these phenotypes is then conditioned by local competition timescales in the diversity that is located in the oligotrophic surface layer on the stratified side of the front. Slow average phytoplankton growth and low primary production levels induced by oligotrophic conditions may lead to longer competition timescales compared to those of the eastern front where the biomass is highest, thereby favoring promoting the coexistence between a large number of phenotypes, including those which do not grow locally. Physical transport is thus shown to act as an "equalizing" effect (Chesson, 2000) by minimizing fitness differences between phenotypes that coexist with a large degree of evenness (Fig. 7) immediately west of the averaged Ushant Front position. The constant flux toward the surface maintains phenotypes that would have unequal fitness in the absence of any transport, and therefore be out of equilibrium; thus increasing local species richness and coexistence occurs, as suggested by the framework of the 'contemporaneous disequilibrium' theory (Richerson et al., 1970).

Noticeably, the simulated diversity maximum comprises three LND phenotypes, with high light optima, that are not accounted for in local diversity elsewhere in our domain (Fig. 10, A). However, following the 'EIE' approach used in our simulations, the presence of those LND phenotypes in significant proportions exclusively within the diversity maximum does not exclude the possibility that either the DCM and/or the well-mixed regions could be a seed for those populations through physical transport although at very low concentrations. Their growth is certainly hindered by more competitive ubiquitous diatoms in the nutrient-replete waters to the east.

Beside those three phenotypes, half of the total diversity (i.e., approximately 35 phenotypes during September) has, surprisingly, positive local net growth in the diversity maximum, although very low monthly mean levels of nutrients (Fig. 15). We hypothesize that short nutrient inputs induced by zonal displacements of maximal gradients at the front with the tidal cycle are sufficient to sustain phytoplanktonic growth, and to allow the development of a few locally adapted species.

4.4. Tidal fronts vs. open ocean fronts

The structure of diversity in frontal areas of the North Atlantic has been the subject of a recent published study (Lévy et al., 2015). In that study, which involves larger scale, open ocean fronts are identified and associated with an increase in phytoplankton diversity. This result is overall consistent with our findings in the coastal Ushant tidal front region. However, in our region, the simulated phytoplankton abundance and species richness maxima are not exactly co-localized as in the case of the open ocean front (Lévy et al., 2015). Our simulated diversity maximum is slightly shifted westward compared to the maximum of phytoplankton biomass and the physical front.

Another major difference between the Ushant tidal front and larger scale fronts is the temporal and spatial scales of variability in frontal structure. Indeed, while frontal structures in the open ocean are generally conserved over a few days, the Ushant tidal front moves zonally with characteristic periods of a few hours (Pingree, 1978). Therefore, the intensity and location of the maximal horizontal density gradient and phytoplankton biomass at the front exhibit some zonal oscillations that are driven by the M2 tide superimposed by fortnightly spring-neap tide cycle (Simpson and Bowers 1979 and 1981; Loder and Greenberg, 1986).

What is the role of tidally-forced variability of a tidal front in establishing or strengthening simulated diversity patterns in the vicinity of the front? Is the shift between the biomass maximum and diversity maximum a specific feature of tidal fronts or is it a feature shared with larger scale geostrophic fronts as well?
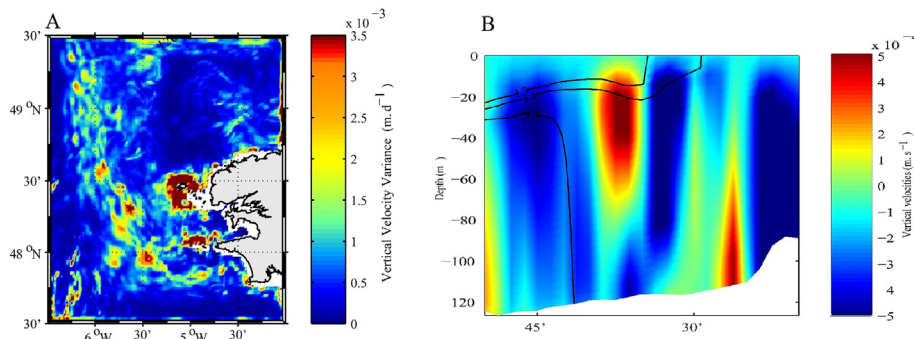
Fig. 14. (A) Time variance of simulated vertical currents (m·d^{-1}) at 10 m during September and (B) Snapshot of vertical currents (m·s^{-1}) on September 1st 2007 along the 48°N transect (Fig. 4, B) with contours of simulated temperature (°C) (black lines).

The magnitude of tidal oscillations (both low/high tide and spring-neap tide cycle) drives the position of the Ushant front (shown in green in Fig. 15), but the time-averaged biomass maximum (i.e., from an Eulerian point of view) is always characterized by sufficient nutrient levels: it is located either east of the front within well-mixed waters (when the front is found at its maximal offshore position) or within the maximal horizontal gradient with nutrient input (when the front is at its more eastern position, see Fig. 15: black isolines vs. green lines). In the absence of nutrient limitation, opportunist microphytoplankton (DIA and LND) quickly outcompete picophytoplankton that has lower growth rates in nutrient-rich waters (Cadier et al., 2017). Imported phenotypes from the DCM through vertical mixing at the front would therefore be less competitive than fast-growing, locally adapted, phenotypes and they are rapidly excluded from diversity calculations in this high biomass region.

Conversely, the time-averaged diversity maximum is alternately within the maximal horizontal gradient with nutrient input (as isopycnals intersect the surface when the front reaches its offshore position) or within the nutrient-depleted region when the front moves eastward (Fig. 15). Therefore, the environmental conditions in the diversity maximum are much more variable than in the biomass maximum, which should increase biodiversity.

Within the maximal nutrient gradient, the nutrient supply induces the growth of several local phenotypes (including in our simulation, three LND phenotypes). Moreover, phenotypes are imported from the DCM by vertical advection and mixing (mostly SNP in our case). Finally, as competitive exclusion happens on longer time-scale on the nutrient-depleted side of the front (Clayton et al., 2013), biodiversity tends to be higher in the eastward limit of the oligotrophic region, west of the

maximum biomass. Then, the time-averaged diversity maximum is the result of locally averaging two unique communities that thrive on either side of the front.

To sum up, regardless of the model structure (i.e., lack of trade-offs in phenotypic traits), a frontal interface between a well-mixed regime and an oligotrophic stratified regime is sufficient to drive the shift between the biomass maximum and diversity maximum by (i) merging phenotypes adapted to both the well-mixed and DCM conditions through transport and (ii) maintaining within the front imported phenotypes by longer time-scale exclusion in the warm, west side of the Ushant Front. Moreover, the tidal variability forced the simulated diversity pattern and increased the diversity west of by generating more unstable environmental conditions at its westward position of the front.

Unfortunately, we do not have observations to determine whether the simulated shift exists in open ocean fronts and this feature has not been specifically investigated in the study of Lévy et al., 2015, although the resolution of 1/54° would have been sufficient. Nonetheless, our results analyze the behavior of a front with specific characteristics: the front separates an oligotrophic region, associated with a DCM, and a more productive well-mixed coastal region, which is not always the case in the open ocean. Further investigations are needed to address the role of these two different regimes on the diversity in frontal zones, as well as the potential impact of the spatio-temporal variability of a tidal front at semi diurnal and spring-neap cycle time scales.

5. Conclusion

In this study, we have investigated how environmental selection and physical processes could drive the spatial patterns of phytoplankton biomass and diversity in a regional, tidal front ecosystem. Our results suggest a zonal shift between biomass and richness maxima mainly driven by the role of physical transport between two contrasted regimes (stratified and oligotrophic vs. well-mixed and productive). A diversity maximum is found in oligotrophic waters slightly west off the front and could be determined by three concurrent factors: (i) horizontal stirring due to zonal displacement of the Ushant Front by tidal amplitudes which homogenize communities (by carrying well-mixed waters species) at the frontal position; (ii) vertical movements on the warm side of the front generates an upward transport and carry DCM species toward the surface and (iii) alternately oligotrophic conditions leading to relatively long interspecific exclusive competition timescales allowing persistence of non locally growing picoplanktonic species transported from the DCM.

Until now, many studies focused on the high productivity of fronts but underlying processes remain uncertain and, to our knowledge, none have been focused on the shaping of the diversity by fronts with a spatial resolution sufficient to resolve mesoscale processes. Therefore, this study is the first to address the shaping of diversity by a tidal front and provides useful contributions to understand the link between a
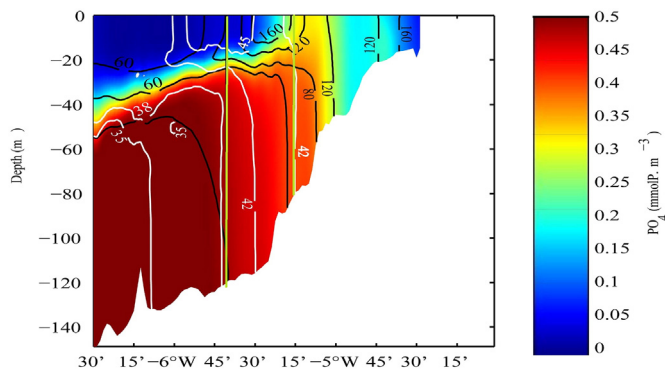

Fig. 15. Monthly (September) averaged vertical structure of phosphate (mmolP·m^{-3}) distribution along the 48°N transect (Fig. 4, B) with contours of averaged phytoplankton biomass (mgC·m^{-3}) in black and local richness (α diversity) in white. Vertical green contour lines show zonal range of variability of the frontal position (defined by the 15 °C isotherm reaching the surface) following spring/neap tide cycle. (For interpretation of the references to color in this figure legend, the reader is referred to the web version of this article.)

frontal circulation and the local diversity measures in the widespread features of a temperate ocean continental shelf.

Sampling mesoscale changes in diversity remains a challenge for marine biologists because of small-scale advection and mixing that occur at high temporal frequencies. A synoptic view of plankton diversity at a regional scale would require simultaneous observations in the study area, implying the deployment of adequate instrumentation to capture high-resolution diversity at high temporal frequencies. Moreover, our study suggests that, given the importance of physical movement compared to the smaller effect of local conditions in the diversity maximum and the relatively low simulated correlation between diversity and biomass, direct links between species richness and environmental factors (mainly light and nutrient distributions) are not straightforward. In this context, modeling tools turn out to be very useful and informative for capturing underlying processes behind simulated patterns. Some limitations of the model, associated with necessary simplifications, still exist and prevent the comprehensive investigations of all aspects contributing to the complex diversity landscape in ecosystem models.

Indeed, some parameterizations preclude the model phytoplankton ecosystem to be fully self-organizing, but they are needed to compensate for the lack of trade-offs between phenotypic traits. Furthermore, to date, there are no sufficient data to include those trade-offs in the model. Moreover, the interactions between species such as symbiosis, mutualism (Hay et al., 2004) or allelopathic effects (Roy and Chattopadhyay, 2007) which are not taken into account and that are likely to affect diversity levels in natural aquatic plankton communities. Also, parasitism and pathogenic organisms are abundant and may constitute a significant source of plankton diversity (Lepère et al., 2008; Skovgaard, 2014). Moreover, trophic interactions and in particular feeding mode (e.g., mixotrophy) and grazer responses to prey variability (i.e., top-down processes) might have a significant effect in shaping phytoplankton diversity. Predation on multiple phytoplankton prey by zooplankton grazers in complex food chains, facilitate the maintenance of high diversity in phytoplankton assemblages (Paine, 1966; Menge and Sutherland, 1976). A better understanding of the consequences of the mesoscale physical environment on predator-prey interactions in plankton would require the use of a model involving further complexity in the zooplankton compartment, through the use of numerous size classes.

Finally, a major problem for modelers remains the evaluation of their results with observational data. Inventories and characterization of natural diversity are increasingly done through the use of genomics (De Vargas et al., 2015; Guidi et al., 2016). Modeling functional diversity as approached in our model is rather based on functional traits regardless of taxonomic considerations. There is therefore a need for a multidisciplinary consensus on integrated microbial/phytoplankton diversity definition if we aim to effectively compare model output with laboratory or field experiments.

Supplementary data to this article can be found online at http://dx.doi.org/10.1016/j.jmarsys.2017.01.004.

Aknowledgments

References

Abraham, E.R., 1998. The generation of plankton patchiness by turbulent stirring. Nature 391, 577–580.

Adjou, M., Bendtsen, J., Richardson, K., 2012. Modeling the influence from ocean transport, mixing and grazing on phytoplankton diversity. Ecol. Model. 225, 19–27.

Auger, P.A., Machu, E., Gorgues, T., Grima, N., Waeles, M., 2015. Comparative study of potential transfer of natural and anthropogenic cadmium to plankton communities in the North-West African upwelling. Sci. Total Environ. 505, 870–888.

Barton, A.D., Dutkiewicz, S., Flierl, G., Bragg, J., Follows, M.J., 2010. Patterns of diversity in marine phytoplankton. Science 327, 1509–1511.

Barton, A.D., Ward, B.A., Williams, R.G., Follows, M.J., 2014. The impact of fine-scale turbulence on phytoplankton community structure. Limnology & Oceanography: Fluids and Environments 4, 34–49.

Bracco, A., Provenzale, A., Scheuring, I., 2000. Mesoscale vortices and the paradox of the plankton. Proceedings. Biological sciences/The Royal Society 267, 1795–1800.

Cadier, M., Gorgues, T., Sourisseau, M., Edwards, C.A., Aumont, O., Marié, L., Memery, L., 2017. Assessing spatial and temporal variability of phytoplankton communities' composition in the Iroise Sea ecosystem (Brittany, France): a 3D modeling approach. Part 1: biophysical control over plankton functional types succession and distribution. J. Mar. Syst. 165, 47–68.

Chase, J.M., Abrams, P.A., Grover, J.P., Diehl, S., Chesson, P., Holt, R.D., Richards, S.A., Nisbet, R.M., Case, T.J., 2002. The interaction between predation and competition: a review and synthesis. Ecol. Lett. 5 (2), 302–315.

Chesson, P., 2000. Mechanisms of maintenance of species diversity. Annu. Rev. Ecol. Syst. 343–366.

Chisholm, S.W., 1992. Phytoplankton size. Springer.

Claustre, H., Kerhervé, P., Marty, J.C., Prieur, L., Videau, C., Hecq, J.-H., 1994. Phytoplankton dynamics associated with a geostrophic front: ecological and biogeochemical implications. J. Mar. Res. 52, 711–742.

Clayton, S., Dutkiewicz, S., Jahn, O., Follows, M.J., 2013. Dispersal, eddies, and the diversity of marine phytoplankton. Limnology & Oceanography: Fluids & Environments 3, 182–197.

De Vargas, C., Audic, S., Henry, N., Decelle, J., Mahé, F., Logares, R., ... Carmichael, M., 2015. Eukaryotic plankton diversity in the sunlit ocean. Science 348 (6237), 1261605.

d'Ovidio, F., De Monte, S., Alvain, S., Dandonneau, Y., Levy, M., 2010. Fluid dynamical niches of phytoplankton types. Proc. Natl. Acad. Sci. U. S. A. 107, 18366–18370.

Dutkiewicz, S., Follows, M.J., Bragg, J.G., 2009. Modeling the coupling of ocean ecology and biogeochemistry. Glob. Biogeochem. Cycles 23.

Echevin, V., Aumont, O., Ledesma, J., Flores, G., 2008. The seasonal cycle of surface chlorophyll in the Peruvian upwelling system: a modelling study. Prog. Oceanogr. 79 (2), 167–176.

Edwards, K.F., Thomas, M.K., Klausmeier, C.A., Litchman, E., 2015. Light and growth in marine phytoplankton: allometric, taxonomic, and environmental variation. Limnol. Oceanogr. 60 (2), 540–552.

Falkowski, P.G., Katz, M.E., Knoll, A.H., Quigg, A., Raven, J.A., Schofield, O., Taylor, F.J., 2004. The evolution of modern eukaryotic phytoplankton. Science 305, 354–360.

Field, C.B., Behrenfeld, M.J., Randerson, J.T., Falkowski, P., 1998. Primary production of the biosphere: integrating terrestrial and oceanic components. Science 281 (5374), 237–240.

Follows, M.J., Dutkiewicz, S., Grant, S., Chisholm, S.W., 2007. Emergent biogeography of microbial communities in a model ocean. Science 315, 1843–1846.

Franks, P.J.S., 1992. Phytoplankton blooms at fronts: patterns, scales and physical forcings mechanisms. Rev. Aquat. Sci. 6, 121–137.

Fuhrman, J.A., Steele, J.A., Hewson, I., Schwalbach, M.S., Brown, M.V., Green, J.L., Brown, J.H., 2008. A latitudinal diversity gradient in planktonic marine bacteria. Proc. Natl. Acad. Sci. 105, 7774–7778.

Gaube, P., McGillicuddy, D.J., Chelton, D.B., Behrenfeld, M.J., Strutton, P.G., 2014. Regional variations in the influence of mesoscale eddies on near-surface chlorophyll. J. Geophys. Res. Oceans 119 (12), 8195–8220.

Gentleman, W., Leising, A., Frost, B., Strom, S., Murray, J., 2003. Functional responses for zooplankton feeding on multiple resources: a review of assumptions and biological dynamics. Deep-Sea Res. II Top. Stud. Oceanogr. 50, 2847–2875.

Gibbons, J.D., Chakraborti, S., 2011. Nonparametric Statistical Inference. fifth ed. Chapman & Hall/CRC Press, Taylor & Francis Group, Boca Raton, FL.

Gohin, F., Druon, J.N., Lampert, L., 2002. A five channel chlorophyll concentration algorithm applied to SeaWiFS data processed by SeaDAS in coastal waters. International journal of remote sensing 23 (8), 1639–1661.

Grover, J.P., 1991. Resource competition in a variable environment: phytoplankton growing according to the variable-internal-stores model. Am. Nat. 811–835.

Guidi, L., Chaffron, S., Bittner, L., Eveillard, D., Larhlimi, A., Roux, S., ... Coelho, L.P., 2016. Plankton networks driving carbon export in the oligotrophic ocean. Nature.

Hay, M.E., Parker, J.D., Burkepile, D.E., Caudill, C.C., Wilson, A.E., Hallinan, Z.P., Chequer, A.D., 2004. Mutualisms and aquatic community structure: the enemy of my enemy is my friend. Annu. Rev. Ecol. Evol. Syst. 175–197.

Hillebrand, H., 2004. Strength slope and variability of marine latitudinal gradients. Mar. Ecol. Prog. Ser. 273, 251–267.

Hillebrand, H., Gruner, D.S., Borer, E.T., Bracken, M.E., Cleland, E.E., Elser, J.J., ... Smith, J.E., 2007. Consumer versus resource control of producer diversity depends on ecosystem type and producer community structure. Proc. Natl. Acad. Sci. 104 (26), 10904–10909.

Holligan, P.M., 1981. Biological implications of fronts on the northwest European continental shelf. Philosophical transactions of the Royal Society of London A: mathematical. Phys. Eng. Sci. 302, 547–562.

Hubbell, S.P., 2001. The Unified Neutral Theory of Biodiversity and Biogeography (MPB-32). Vol. 32. Princeton University Press.

Huisman, J., Weissing, F.J., 2001. Fundamental unpredictability in multispecies competition. Am. Nat. 157, 488–494.

Huston, M., 1979. A general hypothesis of species diversity. Am. Nat. 113, 81–101.

Hutchinson, G.E., 1961. The paradox of the plankton. Am. Nat. 95, 137–145.

Irigoien, X., Huisman, J., Harris, R.P., 2004. Global biodiversity patterns of marine phytoplankton and zooplankton. Nature 429, 863–867.

Jost, L., 2006. Entropy and diversity. Oikos 113 (2), 363–375.

Kiørboe, T., Saiz, E., Viitasalo, M., 1996. Prey switching behaviour in the planktonic copepod *Acartia tonsa*. Mar. Ecol. Prog. Ser. 143, 65–75.

Le Boyer, A., Cambon, G., Daniault, N., Herbette, S., Le Cann, B., Marié, L., Morin, P., 2009. Observations of the Ushant tidal front in September 2007. Cont. Shelf Res. 29, 1026–1037.

Legendre, L., Demers, S., 1984. Towards dynamic biological oceanography and limnology. Can. J. Fish. Aquat. Sci. 41, 2–19.

Legendre, L., Demers, S., Lefaivre, D., 1986. Biological Production at Marine Ergoclines. Elsevier Oceanography Series. Vol. 42 pp. 1–29.

Lepère, C., Domaizon, I., Debroas, D., 2008. Unexpected importance of potential parasites in the composition of the freshwater small-eukaryote community. Appl. Environ. Microbiol. 74, 2940–2949.

Levin, S.A., Paine, T., 1974. Disturbance, patch formation, and community structure. Proc. Natl. Acad. Sci. 71, 2744–2747.

Levy, M., Klein, P., Treguier, A.-M., 2001. Impact of sub-mesoscale physics on production and subduction of phytoplankton in an oligotrophic regime. J. Mar. Res. 59, 535–565.

Levy, M., Jahn, O., Dutkiewicz, S., Follows, M., 2014. Phytoplankton diversity and community structure affected by oceanic dispersal and mesoscale turbulence. Limnology & Oceanography: Fluids and Environments.

Lévy, M., Jahn, O., Dutkiewicz, S., Follows, M.J., d'Ovidio, F., 2015. The dynamical landscape of marine phytoplankton diversity. J. R. Soc. Interface 12, 20150481.

Litchman, E., Klausmeier, C.A., Schofield, O.M., Falkowski, P.G., 2007. The role of functional traits and trade-offs in structuring phytoplankton communities: scaling from cellular to ecosystem level. Ecol. Lett. 10 (12), 1170–1181.

Loder, J.W., Greenberg, D.A., 1986. Predicted positions of tidal fronts in the Gulf of Maine region. Cont. Shelf Res. 6, 397–414.

MacArthur, R.H., Wilson, E.O., 1967. The Theory of Island Biogeography. Princeton University Press.

Mackas, D.L., Denman, K.L., Abbott, M.R., 1985. Plankton patchiness: biology in the physical vernacular. Bull. Mar. Sci. 37, 652–674.

Mariette, V., 1983. Effet des échanges atmosphériques sur la structure thermique marine. Application à des zones du large et une zone côtière:, Brest. Université de Bretagne Occidentale, p. 110.

Martin, A.P., 2003. Phytoplankton patchiness: the role of lateral stirring and mixing. Prog. Oceanogr. 57, 125–174.

McGillicuddy, J.D.J., Dennis, J., 2016. Mechanisms of physical-biological-biogeochemical interaction at the oceanic mesoscale. Mar. Sci. 8.

Menge, B.A., Sutherland, J.P., 1976. Species diversity gradients: synthesis of the roles of predation, competition, and temporal heterogeneity. Am. Nat. 351–369.

Paine, R.T., 1966. Food web complexity and species diversity. Am. Nat. 65–75.

Penven, P., Debreu, L., Marchesiello, P., McWilliams, J.C., 2006. Evaluation and application of the ROMS 1-way embedding procedure to the Central California upwelling system. Ocean Model 12 (1), 157–187.

Perruche, C., Rivière, P., Pondaven, P., Carton, X., 2010. Phytoplankton competition and co-existence: intrinsic ecosystem dynamics and impact of vertical mixing. J. Mar. Syst. 81, 99–111.

Pingree, R.D., 1978. Cyclonic eddies and cross-frontal mixing. J. Mar. Biol. Assoc. UK 58, 955–963.

Pingree, R.D., Holligan, P.M., Mardell, G.T., 1978. The effects of vertical stability on phytoplankton distributions in the summer on the northwest European Shelf. Deep-Sea Res. 25, 1011–1028.

Pommier, T., Canbäck, B., Riemann, L., Boström, K.H., Simu, K., Lundberg, P., Tunlid, A., Hagström, A., 2007. Global patterns pf diversity and community structure in marine bacterioplankton. Mol. Ecol. 16 (4), 867–880.

Prowe, A.F., Pahlow, M., Dutkiewicz, S., Follows, M., Oschlies, A., 2012. Top-down control of marine phytoplankton diversity in a global ecosystem model. Prog. Oceanogr. 101, 1–13.

Ptacnik, R., Solimini, A.G., Andersen, T., Tamminen, T., Brettum, P., Lepisto, L., Willen, E., Rekolainen, S., 2008. Diversity predicts stability and resource use efficiency in natural phytoplankton communities. Proc. Natl. Acad. Sci. U. S. A. 105, 5134–5138.

Richerson, P., Armstrong, R., Goldman, C.R., 1970. Contemporaneous disequilibrium, a new hypothesis to explain the "paradox of the plankton". Proc. Natl. Acad. Sci. 67, 1710–1714.

Ricklefs, R.E., 1987. Community diversity: relative roles of local and regional processes. Science 235, 167–171.

Rivière, P., Pondaven, P., 2006. Phytoplankton size classes competitions at sub-mesoscale in a frontal oceanic region. J. Mar. Syst. 60, 345–364.

Roy, S., Chattopadhyay, J., 2007. Towards a resolution of 'the paradox of the plankton': a brief overview of the proposed mechanisms. Ecol. Complex. 4, 26–33.

Sauterey, B., Ward, B.A., Follows, M.J., Bowler, C., Claessen, D., 2014. When everything is not everywhere but species evolve: an alternative method to model adaptive properties of marine ecosystems. J. Plankton Res., fbu078

Savidge, G., 1976. A preliminary study of the distribution of chlorophyll *a* in the vicinity of fronts in the Celtic and western Irish seas. Estuar. Coast. Mar. Sci. 4, 617–625.

Scheffer, M., Rinaldi, S., Huisman, J., Weissing, F.J., 2003. Why plankton communities have no equilibrium: solutions to the paradox. Hydrobiologia 491, 9–18.

Sedigh Marvasti, S., Gnanadesikan, A., Bidokhti, A.A., Dunne, J.P., Ghader, S., 2016. Challenges in modeling spatiotemporally varying phytoplankton blooms in the Northwestern Arabian Sea and Gulf of Oman. Biogeosciences 13 (4), 1049–1069.

Sharples, J., 2008. Potential impacts of the spring-neap tidal cycle on shelf sea primary production. J. Plankton Res. 30, 183–197.

Shchepetkin, A.F., McWilliams, J.C., 2005. The regional oceanic modeling system (ROMS): a split-explicit, free-surface, topography-following-coordinate oceanic model. Ocean Model 9 (4), 347–404.

Simpson, J.H., Bowers, D., 1979. Shelf sea fronts' adjustments revealed by satellite IR imagery. Nature 280, 648–651.

Simpson, J.H., Bowers, D., 1981. Models of stratification and frontal movement in shelf seas. Deep-Sea Res. I Oceanogr. Res. Pap. 28, 727–738.

Skovgaard, A., 2014. Dirty tricks in the plankton: diversity and role of marine parasitic protists. Acta Protozool. 53, 51.

Sommer, U., 1984. The paradox of the plankton: fluctuations of phosphorus availability maintain diversity of phytoplankton in flow-through cultures. Limnol. Oceanogr. 29, 633–636.

Sun, Y.J., Cho, Y.K., 2010. Tidal front and its relation to the biological process in coastal water. Ocean Sci. J. 45, 243–251.

Tilman, D., 1977. Resource competition between plankton algae: an experimental and theoretical approach. Ecology 58, 338–348.

Tilman, D., 1982. Resource Competition and Community Structure. Princeton University Press.

Vallina, S.M., Follows, M.J., Dutkiewicz, S., Montoya, J.M., Cermeno, P., Loreau, M., 2014a. Global relationship between phytoplankton diversity and productivity in the ocean. Nat. Commun. 5.

Vallina, S.M., Ward, B.A., Dutkiewicz, S., Follows, M.J., 2014b. Maximal feeding with active prey-switching: a kill-the-winner functional response and its effect on global diversity and biogeography. Prog. Oceanogr. 120, 93–109.

Yanagi, T., Ishikawa, K., Inoue, K.I., Susami, S., 1995. Convergence, divergence and vertical velocity at a tidal front in Hiuchi-Nada, Japan. J. Oceanogr. 51 (2), 225–238.